Highly Stable Novel Inorganic Hydrides from Aqueous Electrolysis and Plasma Electrolysis

Randell Mills,* Bala Dhandapani, Ethirajulu Dayalan, Jiliang He, Paresh Ray

BlackLight Power, Inc., 493 Old Trenton Road, Cranbury, NJ 08512, USA

(Received)

ABSTRACT

Each of the ionization of potassium, cesium, and Rb^+ and an electron transfer between two K^+ ions (K^+ / K^+) provide a reaction with a net enthalpy of an integer multiple of the potential energy of atomic hydrogen and catalyze the exothermic formation of lower-energy hydrogen. For each of K^+ / K^+, Rb^+, and cesium, the net enthalpy of reaction of the catalyst is about 27.2 eV, and the lower-energy hydrogen atom catalysis product is predicted to be a highly reactive intermediate which further reacts to form a novel hydride ion $H^-(1/2)$. This ion formed by plasma electrolysis of a K_2CO_3, Rb_2CO_3, or Cs_2CO_3 electrolyte was observed by high resolution visible spectroscopy at 407.0 nm corresponding to its predicted binding energy of 3.05 eV. Furthermore, novel inorganic hydride compounds such as $KH\,KHCO_3$ and KH were isolated following the electrolysis of a K_2CO_3 electrolyte and identified by ToF-SIMS. The existence of novel hydride ions was determined using X-ray photoelectron spectroscopy and proton nuclear magnetic resonance spectroscopy. Applications include high voltage batteries.

KEYWORDS: plasma electrolysis, novel hydride ion, highly stable hydride compounds, high voltage battery, catalytic hydride synthesis

* rmills@blacklightpower.com

1. INTRODUCTION

1.1. Background

Evidence of the changing landscape for automobiles can be found in the recent increase in research into the next generation of automobiles. But, the fact that there is no clear front-runner in the technological race to replace the internal combustion (IC) engine can be attested to by the divergent approaches taken by the major automobile companies. Programs include various approaches to hybrid vehicles, alternative fueled vehicles such as dual-fired engines that can run on gasoline or compressed natural gas, and a natural gas-fired engine. Serious efforts are also being put into a number of alternative fuels such as ethanol, methanol, propane, and reformulated gasoline. To date, the most favored approach is an electric vehicle based on fuel cell technology or advanced battery technology such as sodium nickel chloride, nickel-metal hydride, and lithium-ion batteries [1]. Although billions of dollars are being spent to develop an alternative to the IC engine, there is no technology in sight that can match the specifications of an IC engine system [2].

Fuel cells have advantages over the IC engine because they convert hydrogen to water at about 70% efficiency when running at about 20% below peak output [3]. But, hydrogen is difficult and dangerous to store. Cryogenic, compressed gas, and metal hydride storage are the main options. In the case of cryogenic storage, liquefaction of hydrogen requires an amount of electricity which is at least 30% of the lower heating value of liquid hydrogen [4]. Compressed hydrogen, and metal hydride storage are less viable since the former requires an unacceptable volume, and the latter is heavy and has difficulties supplying hydrogen to match a load such as a fuel cell [4]. The main challenge with hydrogen as a replacement to gasoline is that a hydrogen production and refueling infrastructure would have to be built. Hydrogen may be obtained by reforming fossil fuels. However, in practice fuel cell vehicles would probably achieve only 10 to 45 percent efficiency because the process of reforming fossil fuel into hydrogen and carbon dioxide requires energy [3]. Presently, fuel cells are also impractical due to their high cost as well as the lack of inexpensive reforming technology [5].

In contrast, batteries are attractive because they can be recharged wherever electricity exists which is ubiquitous. The cost of mobile energy from a battery powered car may be less than that from a fossil fuel powered car. For example, the cost of energy per mile of a nickel metal hydride battery powered car is 25% of that of a IC powered car [6]. However, current battery technology is trying to compete with something that it has little chance of imitating. Whichever battery technology proves to be superior, no known electric power plant will match the versatility and power of an internal combustion engine. A typical IC engine yields more

than 10,000 watt-hours of energy per kilogram of fuel, while the most promising battery technology yields 200 watt-hours per kilogram [2].

A high voltage battery would have the advantages of much greater power and much higher energy density. The limitations of battery chemistry may be attributed to the binding energy of the anion of the oxidant. For example, the 2 volts provided by a lead acid cell is limited by the 1.46 eV electron affinity of the oxide anion of the oxidant PbO_2. An increase in the oxidation state of lead such as $Pb^{2+} \rightarrow Pb^{3+} \rightarrow Pb^{4+}$ is possible in a plasma. Further oxidation of lead could also be achieved in theory by electrochemical charging. However, higher lead oxidation states are not achievable because the oxide anion required to form a neutral compound would undergo oxidation by the highly oxidized lead cation. An anion with an extraordinary binding energy is required for a high voltage battery. One of the highest voltage batteries known is the lithium fluoride battery with a voltage of about 6 volts. The voltage can be attributed to the higher binding energy of the fluoride ion. The electron affinity of halogens increases from the bottom of the Group VII elements to the top. Hydride ion may be considered a halide since it possess the same electronic structure. And, according to the binding energy trend, it should have a high binding energy. However, the binding energy is only 0.75 eV which is much lower than the 3.4 eV binding energy of a fluoride ion.

1.2. Catalysis of Hydrogen to Form Novel Hydrides

Atomic hydrogen may undergo a catalytic reaction with certain atomized elements and ions which singly or multiply ionize at integer multiples of the potential energy of atomic hydrogen, $m \cdot 27.2\ eV$ wherein m is an integer. The theory and supporting data were given previously [7-42]. The reaction involves a nonradiative energy transfer to form a hydrogen atom, "hydrino" designated by $H(1/p)$, that is lower in energy than unreacted atomic hydrogen that corresponds to a fractional principal quantum number ($n = \frac{1}{p} = \frac{1}{\text{integer}}$ replaces the well known parameter n = integer in the Rydberg equation for hydrogen excited states). A number of independent experimental observations lead to the conclusion that atomic hydrogen can exist in fractional quantum states that are at lower energies than the traditional "ground" ($n = 1$) state. Prior related studies that support the possibility of a novel reaction of atomic hydrogen which produces a chemically generated or assisted plasma (rt-plasma) and produces novel hydride compounds include extreme ultraviolet (EUV) spectroscopy [12-14,16,18-25,28-30], characteristic emission from catalysis and the hydride ion products [15-20], lower-energy atomic and molecular hydrogen emission [12-14,24], plasma formation [15,16,18-22,28,29,31,32], Balmer α line broadening [13,15,16,21,22,24-26], elevated electron temperature [13,24], anomalous plasma afterglow

duration [31,32], power generation [13,15,21-24,26-28,39], and analysis of chemical compounds [33-39]. Furthermore, mobility and spectroscopy data of individual electrons in liquid helium shows direct experimental confirmation that electrons may have fractional principal quantum energy levels [11].

An atomic catalytic system to produce a rt-plasma involves helium ions. The second ionization energy of helium is 54.4 eV [43]; thus, the ionization reaction of He^+ to He^{2+} has a net enthalpy of reaction of 54.4 eV which is equivalent to $2 \cdot 27.2\ eV$. Thus, it may serve as a catalyst to form $H(1/3)$. The products of the catalysis reaction may accept energy nonradiatively in multiples of the potential energy of atomic hydrogen and may further serve as catalysts. Thus, once a hydrino atom is formed by a catalyst, further catalytic transitions $n = \frac{1}{3} \rightarrow \frac{1}{4}$, $\frac{1}{4} \rightarrow \frac{1}{5}$, and so on occur to a substantial extent.

Extreme ultraviolet (EUV) spectra recorded on microwave discharges of helium with 2% hydrogen were previously reported [12,13,24]. Novel emission lines were observed with energies of $q \cdot 13.6\ eV$ where $q = 1,2,3,4,6,7,8,9,11,12$ or these lines inelastically scattered by helium atoms wherein 21.2 eV was absorbed in the excitation of $He(1s^2)$ to $He(1s^1 2p^1)$. These lines were identified as hydrogen transitions to electronic energy levels below the "ground" state corresponding to fractional quantum numbers. The hydrino catalysis product may further react with a source of electrons to form the corresponding hydride ion.

Each of K^+/K^+, Rb^+, Cs, and Ar^+ are predicted to catalyze hydrogen to form $H\left[\frac{a_H}{2}\right]$ which reacts with an electron to form $H^-(1/2)$. A potassium atom is predicted to catalyze hydrogen to form $H\left[\frac{a_H}{4}\right]$ which reacts with an electron to form $H^-(1/4)$. Several studies including EUV and high resolution visible spectroscopy on rt-plasmas from several salt or metal catalysts confirmed the catalyst mechanism and the predicted novel hydride ions.

$H^-(1/2)$, the hydride ion catalyst product of K^+/K^+ or Rb^+, was observed by high resolution visible spectroscopy as a broad peak at 407.00 nm with a FWHM of 0.14 nm corresponding to its predicted binding energy of 3.0468 eV. From the electron g factor, bound-free hyperfine structure lines of $H^-(1/2)$ were predicted with energies E_{HF} given by $E_{HF} = j^2 3.0056\ X\ 10^{-5} + 3.0575\ eV$ (j is an integer) as an inverse Rydberg-type series that converges at increasing wavelengths and terminates at 3.0575 eV—the hydride spin-pairing energy plus the binding energy. The high resolution visible plasma emission spectra in the region of 400.0 nm to 406.0 nm matched the predicted emission lines for $j = 1$ to $j = 37$ [16] to within a 1 part per 10^5.

Further exemplary studies include:

1.) the observation of continuum state emission of Cs^{2+} and Ar^{2+} at 53.3 *nm* and 45.6 *nm*, respectively, with the absence of the other corresponding Rydberg series of lines from these species which confirmed the resonant nonradiative energy transfer of 27.2 *eV* from atomic hydrogen to the catalysts atomic *Cs* or Ar^+ [20],

2.) the spectroscopic observation of the predicted hydride ion $H^-(1/2)$ of hydrogen catalysis by either *Cs* atom or Ar^+ catalyst at 407.0 *nm* corresponding to its predicted binding energy of 3.05 *eV* [15-17, 20],

3.) the observation of characteristic emission from K^{3+} which confirmed the resonant nonradiative energy transfer of $3 \cdot 27.2$ *eV* from atomic hydrogen to atomic *K* [19],

4.) the spectroscopic observation of the predicted $H^-(1/4)$ ion of hydrogen catalysis by *K* catalyst at 110 *nm* corresponding to its predicted binding energy of 11.2 *eV* [19],

5.) the observation of characteristic emission from Rb^{2+} which confirmed the resonant nonradiative energy transfer of 27.2 *eV* from atomic hydrogen to Rb^+ [18],

6.) the spectroscopic observation of the predicted $H^-(1/2)$ ion of hydrogen catalysis by Rb^+ catalyst at 407.0 *nm* corresponding to its predicted binding energy of 3.05 *eV* [15-18],

7.) the high resolution visible spectroscopic observation from rt-plasmas of the predicted $H^-(1/2)$ ion of hydrogen catalysis by each of K^+/K^+, Rb^+, *Cs*, and Ar^+ at 407.0 *nm* corresponding to its predicted binding energy of 3.05 *eV* [15-20],

The formation of novel compounds having hydrino hydride ions would be substantial evidence supporting catalysis of hydrogen as the mechanism of observed rt-plasmas and further support the spectroscopic identification of $H^-(1/p)$ (p is an integer). Compounds containing novel hydride ions have been isolated as products of the reaction of atomic hydrogen with atoms and ions identified as catalysts in previously reported EUV studies [33-39]. The novel hydride compounds were identified analytically by techniques such as time of flight secondary ion mass spectroscopy, X-ray photoelectron spectroscopy, and ^1H nuclear magnetic resonance spectroscopy. For example, the time of flight secondary ion mass spectroscopy showed a large hydride peak in the negative spectrum. The X-ray photoelectron spectrum showed large metal core level shifts due to binding with the hydride as well as novel hydride

peaks. The ^1H nuclear magnetic resonance spectrum showed significantly upfield-shifted peaks which corresponded to and identified novel hydride ions [33].

In this article we report that novel inorganic hydride compounds having the formula $KH\,KHCO_3$ and KH were isolated from an aqueous K_2CO_3 electrolytic cell reactor. KH was stable at elevated temperature (600°C). Inorganic hydride clusters $K[KH\,KHCO_3]_n$ were identified by positive ToF-SIMS of $KH\,KHCO_3$. The negative ToF-SIMS was dominated by hydride ion. The positive and negative ToF-SIMS of KH showed essentially K^+ and H^- only, respectively. A hydride ion with a binding energy of 22.8 eV has been observed by X-ray photoelectron spectroscopy (XPS) of $KH\,KHCO_3$ having upfield shifted solid state magic-angle spinning proton nuclear magnetic resonance (^1H MAS NMR) peaks. Moreover, a polymeric structure is indicated by Fourier transform infrared (FTIR) spectroscopy. Hydride ions with binding energies of 22.8 eV and 69.2 eV have been observed by XPS of KH. $H^-(1/2)$, the predicted hydride ion product with each of K^+ / K^+, Rb^+, and Cs as the catalyst, has a binding energy of 3.05 eV corresponding to a 407.0 nm emission that was observed by high resolution visible spectroscopy on the emission from plasma electrolysis cells.

1.3. Hydride Ion Battery

The discovery of novel hydride ions with high binding energies has implications for a new field of hydride chemistry with applications such as a high voltage battery. Such extremely stable hydride ions may stabilize positively charged ions in an unprecedented highly charged state. A battery may be possible having projected specifications and environmental advantages that may be competitive with the internal combustion engine.

Hydride ions having extraordinary binding energies may stabilize a cation M^{z+} in an extraordinarily high oxidation state such as +2 in the case of lithium. Thus, these hydride ions may be used as the basis of a high voltage battery of a rocking chair design wherein the hydride ion moves back and forth between the cathode and anode half cells during discharge and charge cycles. Exemplary reactions for a cation M^{z+} are:

Cathode reaction:

$$MH_x + e^- \rightarrow MH_{x-1} + H^- \tag{1}$$

Anode reaction:

$$MH_{x-2} + H^- \rightarrow MH_{x-1} + e^- \quad (2)$$

Overall reaction:

$$MH_x + MH_{x-2} \rightarrow 2MH_{x-1} \quad (3)$$

2. EXPERIMENTAL

2.1. Synthesis

2.1.1. Potassium Hydride Potassium Hydrogen Carbonate, KH $KHCO_3$, Synthesis with an Electrolytic Cell

An electrolytic cell comprising a K_2CO_3 electrolyte, a nickel wire cathode, and platinized titanium anodes was used to synthesize the $KH\,KHCO_3$ sample. Briefly, the cell vessel comprised a 37.85 liter (83.82 cm x 38.1 cm) Nalgene tank. An outer cathode comprised 5000 meters of 0.5 mm diameter clean, cold drawn nickel wire (NI 200 0.5 mm, HTN36NOAG1, A-1 Wire Tech, Inc., 840-39th Ave., Rockford, Illinois, 61109) wound on a polyethylene cylindrical support. A central cathode comprised 5000 meters of the nickel wire wound in a toroidal shape. The central cathode was inserted into a cylindrical, perforated polyethylene container that was placed inside the outer cathode with an anode array between the central and outer cathodes. The anode comprised an array of 15 platinized titanium anodes (ten - Engelhard Pt/Ti mesh 4.06 cm x 20.32 cm with one 1.91 cm x 17.78 cm stem attached to the 4.06 cm side plated with 100 U Pt series 3000; and 5 - Engelhard 2.54 cm diameter x 20.32 cm length titanium tubes with one 1.91 cm x 17.78 cm stem affixed to the interior of one end and plated with 100 U Pt series 3000). Before assembly, the anode array was cleaned in 3 M HCl for 5 minutes and rinsed with distilled water. The cathode was cleaned by placing it in a tank of 0.57 M K_2CO_3/3% H_2O_2 for 6 hours and then rinsing it with distilled water. The anode was placed in the support between the central and outer cathodes, and the electrode assembly was placed in the tank containing electrolyte. The electrolyte solution comprised 28 liters of 0.57 M K_2CO_3 (Alfa K_2CO_3 99%). Electrolysis was performed at 20 amps constant current with a constant current (± 0.02%) power supply for 15 months with water add-back to maintain the 28 liters constant.

Samples were isolated from the electrolytic cell by concentrating the K_2CO_3 electrolyte about six fold using a rotary evaporator at 50°C until a yellow white polymeric suspension formed. Precipitated crystals of the suspension were then grown over three weeks by allowing

the saturated solution to stand in a sealed round bottom flask at 25°C. Control samples utilized in the following experiments contained K_2CO_3 (99%), $KHCO_3$ (99.99%), KNO_3 (99.99%), KI (99.99%), KOH (99.9%), and KH (99%).

2.1.2. Potassium Hydrino Hydride, KH, Synthesis with an Electrolytic Cell

An electrolytic cell comprising a K_2CO_3 electrolyte, a nickel wire cathode, and platinized titanium anodes was also used to synthesize potassium hydride, KH. The cell was equivalent to that described *supra.* except that it lacked the additional central cathode.

After 3 months of operation, the cathode wire obtained a graphite colored coating. The cathode was placed in 37.85 liter (83.82 cm x 38.1 cm) Nalgene tank of 0.57 M K_2CO_3/3% H_2O_2 for 6 hours. A very vigorous exothermic reaction was observed during the six hours. The cathode was removed and placed in a second 37.85 liter (83.82 cm x 38.1 cm) Nalgene tank of distilled water. NiO was observed to precipitate in the tank containing 0.57 M K_2CO_3/3% H_2O_2. The coat was observed to be removed from the cathode when it was pulled from the distilled water bath. A white polymeric solid floated to the top of the water bath over 2 weeks. The solid was collected by scooping it with a 250 ml beaker. The polymeric material was stable in water indefinitely (over a year with no observable change). The material was pure white and appeared like cotton suspended in water. Other samples were obtained which were thin films. The density was less than that of water. The material was observed to be weakly ferromagnetic. It collapsed along the magnet field lines and was attracted to a magnet in solution. It could be pulled out of water with a strong magnet. It was poured onto an evaporation dish, dried, and analyzed.

2.2. ToF-SIMS Characterization

The crystalline samples were sprinkled onto the surface of double-sided adhesive tapes and characterized using a Physical Electronics TFS-2000 ToF-SIMS instrument. The primary ion gun utilized a $^{69}Ga^+$ liquid metal source. In order to remove surface contaminants and expose a fresh surface, the samples were sputter cleaned for 30 seconds using a $40\,\mu m$ X $40\,\mu m$ raster. The aperture setting was 3, and the ion current was 600 pA resulting in a total ion dose of 10^{15} $ions/cm^2$.

During acquisition, the ion gun was operated using a bunched (pulse width 4 ns bunched to 1 ns) 15 kV beam [44-45]. The total ion dose was 10^{12} $ions/cm^2$. Charge neutralization was active, and the post accelerating voltage was 8000 V. Three different

regions on each sample of $(12\mu m)^2$, $(18\mu m)^2$, and $(25\mu m)^2$ were analyzed. The positive and negative SIMS spectra were acquired. Representative post sputtering data is reported.

2.3. XPS Characterization

A series of XPS analyses were made on the crystalline samples each mounted on a silicon wafer using a Scienta 300 XPS Spectrometer. The fixed analyzer transmission mode and the sweep acquisition mode were used. A survey spectrum was obtained over the region $E_b = 0\ eV$ to $1200\ eV$. The primary element peaks allowed for the determination of all of the elements present in each sample isolated from the K_2CO_3 electrolyte. The survey spectrum also detected shifts in the binding energies of potassium and oxygen which had implications as to the identity of the compound containing the elements. A high resolution XPS spectrum was also obtained of the low binding energy region ($E_b = 0\ eV$ to $100\ eV$) to determine the presence of novel XPS peaks. The step energy in the survey scan was $0.5\ eV$, and the step energy in the high resolution scan was $0.15\ eV$. In the survey scan, the time per step was 0.4 seconds, and the number of sweeps was 4. In the high resolution scan, the time per step was 0.3 seconds, and the number of sweeps was 30. $C\ 1s$ of trace graphitic carbon contamination at $284.6\ eV$ was used as the internal standard.

2.4. NMR Spectroscopy

^1H MAS NMR was performed on the crystalline samples. The data were obtained on a custom built spectrometer operating with a Nicolet 1280 computer. Final pulse generation was from a tuned Henry radio amplifier. The ^1H NMR frequency was 270.6196 MHz. A 2 μsec pulse corresponding to a 15° pulse length and a 3 second recycle delay were used. The window was $\pm 31\ kHz$. The spin speed was 4.5 kHz. The number of scans was 1000. The offset was 1527.12 Hz, and the magnetic flux was 6.357 T. Chemical shifts were referenced to external TMS.

2.5. FTIR Spectroscopy

Samples were transferred to an infrared transmitting substrate and analyzed by FTIR spectroscopy using a Nicolet Magna 550 FTIR Spectrometer with a NicPlan FTIR microscope. The number of scans was 500 for both the sample and background. The resolution was 8 cm^{-1}. A dry air purge was applied.

2.6. Thermal Decomposition with Analysis by Mass Spectroscopy

Mass spectroscopy was performed on the gases released from the thermal decomposition of the samples. One end of a 4 mm ID fritted capillary tube containing about 5 mg of sample was sealed with a 6.35 mm in. Swagelock union and plug (Swagelock Co., Solon, OH). The other end was connected directly to the sampling port of a Dycor System 1000 Quadrapole Mass Spectrometer (Model D200MP, Ametek, Inc., Pittsburgh, PA with a HOVAC Dri-2 Turbo 60 Vacuum System). The capillary was heated with a Nichrome wire heater wrapped around the capillary. The mass spectrum was obtained at the ionization energy of 70 eV at a sample temperature of 600°C with the detection of hydrogen indicated by a $m/e = 2$ peak.

The control hydrogen gas was ultrahigh purity (MG Industries).

2.7. High Resolution Visible Spectroscopy of Plasma Electrolysis Cells

The plasma electrolysis cell shown in Fig. 1 comprised a 800 ml glass beaker covered with a Teflon lid with a gas outlet and 4 penetrations for electrodes, a thermometer, and a circulating water cold finger for cooling. The electrolyte comprised 600 ml of 0.15 M aqueous $Na_2CO_3 \cdot H_2O$ (99.5% Alfa Aesar), K_2CO_3 (99% Fluka), Rb_2CO_3 (99% Alfa Aesar), or Cs_2CO_3 (99% Alfa Aesar). The cathode that was sufficiently durable for long duration electrolysis was a 0.3 cm diameter tungsten rod with 3 cm immersed in the electrolyte. To eliminate the possibility of tungsten emission lines in the region of 407 nm, the experiments were repeated with the tungsten cathode replaced by a 0.1 cm diameter platinum wire cathode. The anode was a 20 cm^2 platinum wire gauze. The high voltage electrolysis power was supplied by two Xantrex XFR 100-28 (0-100 V, 0-28 A) DC power supplies connected in series. The electrolysis was carried out at about 160 V and about 3A. Using water cooling, the cell was maintained under bright cathode plasma conditions corresponding to a temperature of about 90°C.

The high resolution visible spectrum of each electrolysis plasma was recorded over the range $400 - 410\ nm$ to search for the $407.0\ nm$ emission of $H(1/2)$. Other regions were scanned to eliminate known elements as discussed in Sec. IIIG. The plasma emission was fiber-optically coupled through a 220F matching fiber adapter positioned at the wall of the beaker just opposite to the cathode to a high resolution visible spectrometer with a resolution of $\pm 0.006\ nm$ over the spectral range $190 - 860\ nm$. The spectrometer was a Jobin Yvon Horiba 1250 M with 2400 groves/mm ion-etched holographic diffraction grating. The entrance and exit slits were set to $20\ \mu m$. The spectrometer was scanned between $400 - 410\ nm$ using a

0.001 *nm* step size. The signal was recorded by a PMT with a stand alone high voltage power supply (950 V) and an acquisition controller. The data was obtained in a single accumulation with a 1 second integration time.

In addition, a low resolution spectrum of each electrolysis plasma was recorded over the range 400 – 900 *nm* to identify the emitting species such as hydrogen and alkali species. The spectrometer system comprised a 100 μm optical fiber and visible spectrometer (Ocean Optics S2000). To correct for the nonuniform response of the spectrometer system as a function of wavelength, the system was calibrated against a reference light source (Ocean Optics LS-1-CAL), and the count rate data at each wavelength was corrected by the spectral calibration factor.

3. RESULTS AND DISCUSSION

3.1. ToF-SIMS

3.1.1. ToF-SIMS of Potassium Hydride Potassium Hydrogen Carbonate, KH $KHCO_3$, Electrolytic Cell Sample

The positive ToF-SIMS spectrum obtained from the $KHCO_3$ control is shown in Figs. 2 and 3. In addition, the positive ToF-SIMS of a sample isolated from the electrolytic cell is shown in Figs. 4 and 5. The respective hydride compounds and mass assignments appear in Table I. In both the control and electrolytic samples, the positive ion spectrum are dominated by the K^+ ion. Two series of positive ions $\{K[K_2CO_3]_n^+ \quad m/z = (39 + 138n)$ and $K_2OH[K_2CO_3]_n^+ \quad m/z = (95 + 138n)\}$ are observed in the $KHCO_3$ control. Other peaks containing potassium include KC^+, $K_xO_y^+$, $K_xO_yH_z^+$, KCO^+, and K_2^+. However, in the electrolytic cell sample, three new series of positive ions are observed at $\{K[KH\,KHCO_3]_n^+ \quad m/z = (39 + 140n)$, $K_2OH[KH\,KHCO_3]_n^+ \quad m/z = (95 + 140n)$, and $K_3O[KH\,KHCO_3]_n^+ \quad m/z = (133 + 140n)\}$. These ions correspond to inorganic clusters containing novel hydride combinations (i.e. $KH\,KHCO_3$ units plus other positive fragments).

The comparison of the positive ToF-SIMS spectrum of the $KHCO_3$ control with the electrolytic cell sample shown in Figs. 2 and 3 and Figs. 4 and 5, respectively, demonstrates that the $^{39}K^+$ peak of the electrolytic cell sample may saturate the detector and give rise to a peak that is atypical of the natural abundance of ^{41}K. The natural abundance of ^{41}K is 6.7%; whereas, the observed ^{41}K abundance from the electrolytic cell sample is 57%. This atypical abundance was also confirmed using Electrospray-Ionization-Time-of-Flight-Mass-

Spectroscopy (ESIToFMS). The high resolution mass assignment of the $m/z = 41$ peak of the electrolytic sample was consistent with ^{41}K, and no peak was observed at $m/z = 42.98$ ruling out $^{41}KH_2^+$. Moreover, the natural abundance of ^{41}K was observed in the positive ToF-SIMS spectra of $KHCO_3$, KNO_3, and KI standards that were obtained with an ion current such that the ^{39}K peak intensity was an order of magnitude higher than that given for the electrolytic cell sample. The saturation of the ^{39}K peak of the positive ToF-SIMS spectrum by the electrolytic cell sample is indicative of a unique crystalline matrix [46].

The negative ToF-SIMS spectrum ($m/e = 0 - 50$) of the $KHCO_3$ (99.99%) sample and the negative ToF-SIMS spectrum ($m/e = 0 - 30$) of the electrolytic cell sample are shown in Figs. 6 and 7, respectively. The negative ion ToF-SIMS of the electrolytic cell sample was dominated by H^-, O^-, and OH^- peaks. A series of nonhydride containing negative ions $\{KCO_3[K_2CO_3]_n \; m/z = (99+138n)\}$ was also present which implies that H_2 was eliminated from $KHKHCO_3$ during fragmentation of the compound $KHKHCO_3$. Comparing the H^- to O^- ratio of the electrolytic cell sample to that of the $KHCO_3$ control sample, the H^- peak was about an order of magnitude higher in the electrolytic cell sample.

3.1.2. ToF-SIMS of Potassium Hydrino Hydride, KH, Electrolytic Cell Sample

The positive ToF-SIMS spectrum obtained from the KH electrolytic cell sample is shown in Fig. 8. The positive spectrum was dominated by the potassium peak K^+ $m/z = 39$ followed by the proton peak. Small silicon, sodium, and hydrocarbon fragment peaks such as $C_2H_3^+$ $m/z = 27$ and $C_2H_5^+$ $m/z = 29$, K_2^+ $m/z = 87$, $K(KO)^+$ $m/z = 94$, and $K(KOH)^+$ $m/z = 95$ were also observed.

The positive spectrum of the $KHCO_3$ control shown in Figs. 2 and 3 was also dominated by the potassium peak K^+ $m/z = 39$. Two series of positive ions $\{K[K_2CO_3]_n \; m/z = (39+138n)$ and $K_2OH[K_2CO_3]_n \; m/z = (95+138n)\}$ were observed in the $KHCO_3$ control. Other peaks containing potassium included KC^+ $m/z = 51$, $K_xO_y^+$, $K_xO_yH_z^+$, KCO^+ $m/z = 67$, and K_2^+ $m/z = 78$.

The negative ion ToF-SIMS of KH shown in Fig. 9 was dominated by H^-. O^- $m/z = 16$ and OH^- $m/z = 17$ dominated the negative ion ToF-SIMS of the $KHCO_3$ control as shown in Fig. 6. These peaks were present in the case of KH, but they were very small in comparison to the $KHCO_3$ control. For both samples smaller hydrocarbon fragment peaks such as C^- $m/z = 12$ and CH^- $m/z = 13$ were observed. A series of negative ions $\{KCO_3[K_2CO_3]_n \; m/z = (99+138n)\}$ was also present in the control which were not observed

in the KH sample. A hydride peak probably due to OH^- $m/z = 17$ which was significantly smaller than the O^- $m/z = 16$ peak was observed in the control.

3.2. XPS

3.2.1. XPS of Potassium Hydride Potassium Hydrogen Carbonate, KH $KHCO_3$, Electrolytic Cell Sample

The 0 to 80 eV binding energy region of a high resolution XPS spectrum of the $KH\,KHCO_3$ electrolytic cell sample is shown in Fig. 10. The XPS survey spectrum the $KH\,KHCO_3$ electrolytic cell sample with the primary elements identified is shown in Fig. 11. No elements were present in the survey scans which can be assigned to peaks in the low binding energy region with the exception of a small variable contaminant of sodium at 63 eV and 31 eV, potassium at 16.2 eV and 32.1 eV, and oxygen at 23 eV. Accordingly, any other peaks in this region must be due to novel species. The $K\,3s$ and $K\,3p$ are shown in Fig. 10 at 16.2 eV and 32.1 eV, respectively. A weak $Na\ 2s$ is observed at 63 eV. The $O\ 2s$ which is weak compared to the potassium peaks of K_2CO_3 is typically present at 23 eV, but is broad or obscured in Fig. 10.

Peaks centered at 22.8 eV and 38.8 eV which do not correspond to any other primary element peaks were observed. The relative intensities and shift of each peak match $K\,3s$ and $K\,3p$ peaks shifted to higher binding energies. Hydrogen is the only element which does not have primary element peaks; thus, it is the only candidate to produce the shifted peaks. These peaks may be shifted by a highly binding hydride ion with a binding energy of 22.8 eV as observed in other compounds by Mills et al. [15-20, 33-39] that bonds to potassium $K\,3p$ and shifts the peak to this energy. In this case, the $K\,3s$ is similarly shifted. These peaks were not present in the case of the XPS of matching samples isolated from an identical electrolytic cell except that Na_2CO_3 replaced K_2CO_3 as the electrolyte.

XPS further confirmed the ToF-SIMS data by showing shifts of the primary elements. The splitting of the principal peaks of the survey XPS spectrum is indicative of multiple forms of bonding involving the atom of each split peak. For example, the XPS survey spectrum shown in Fig. 11 shows extraordinary potassium and oxygen peak shifts. All of the potassium primary peaks are shifted to about the same extent as that of the $K\,3s$ and $K\,3p$. In addition, extraordinary $O\ 1s$ peaks of the electrolytic cell sample were observed at 537.5 eV and 547.8 eV; whereas, a single $O\ 1s$ was observed in the XPS spectrum of K_2CO_3 at 532.0 eV. The results are not due to uniform charging as the internal standard $C\ 1s$ remains the same at 284.6 eV. The results are not due to differential charging because the peak shapes of carbon

and oxygen are normal, and no tailing of these peaks was observed. The binding energies of the K_2CO_3 control and the $KH\,KHCO_3$ electrolytic cell sample are shown in Table II. The range of literature [47] values of the binding energies of the peaks of interest are given in the final row of Table II. The $K\,3p$, $K\,3s$, $K\,2p_{3/2}$, $K\,2p_{1/2}$, and $K\,2s$ XPS peaks and the $O\,1s$ XPS peaks shifted to an extent greater than those of known compounds may correspond to and identify $KH\,KHCO_3$.

3.2.2. XPS of Potassium Hydrino Hydride, KH, Electrolytic Cell Sample

The XPS survey scan of the KH electrolytic cell sample is shown in Fig. 12. $C\,1s$ at 284.5 eV was used as the internal standard for the KH sample and the control K_2CO_3. The major species present in the control are potassium and carbon and oxygen. The major species present in the KH sample was potassium. Large silicon, oxygen and graphitic and hydrocarbon carbon peaks were also seen that originated from the silicon wafer sample mount. Nitrogen was present, and trace magnesium and sodium may be present. The identifying peaks of the primary elements and their binding energies are: $Na\,1s$ at 1072.2 eV, $O\,1s$ at 532.0 eV, $Na\,KL_{23}L_{23}$ at 496.6 eV, $N\,1s$ at 399.3 eV, $K\,2s$ at 377.2 eV, $Mg\,KL_{23}L_{23}$ at 305.9 eV, $K\,2p_{1/2}$ at 295.4 eV, $K\,2p_{3/2}$ at 292.5 eV, $C\,1s$ at 285.5 and 284.6 eV, $Si\,2p_{3/2}$ at 156.7 eV and 153.4 eV, $Si\,2s$ at 105.7 eV and 102.1 eV, and $Mg\,2s$ at 88.5 eV.

No elements were present in the survey scan which could be assigned to peaks in the low binding energy region with the exception of the $K\,3p$ at 16.8 eV, $K\,3s$ at 33.0 eV, $O\,2s$ at 26.2 eV, and $Mg\,2p$ at 49.6 eV. Accordingly, any other peaks in this region must be due to novel species. The 0-80 eV binding energy region of a high resolution XPS spectrum of the KH electrolytic cell sample is shown in Fig. 13. Peaks of interest were observed in the valance band at 3.8 eV, 9.95 eV, and 13.7 eV which may be due to nitrogen, carbon, and oxygen, but the assignment can not be made with certainty. A 62.8 peak may be assigned to $Na\,2s$. However, no peak is detectable above baseline at 29.8 eV which corresponds to $Na\,2p_{1/2}$. Since the intensity of the $Na\,2p_{1/2}$ peak is less than $Na\,2s$, and the $Na\,2s$ peak is weak, the $Na\,2p_{1/2}$ may not be seen. So, the assignment is uncertain. Novel peaks were observed in the KH sample at 19.5 eV, 36.0 eV, and 68.0 eV. The 68.0 eV peak may be assigned to $Ni\,3p$, but the shape is incorrect. And, if the $Ni\,2p_{3/2}$ at about 860 eV is present, it is smaller than the proposed $Ni\,3p$. Thus, the 68.0 eV can not be assigned to $Ni\,3p$.

The XPS peaks at 19.5 eV, 36.0 eV, and 68.0 eV do not correspond to any other primary element peaks. The 68.0 eV peak may correspond to a hydride ion with a binding energy of 69.2 eV as observed in other compounds by Mills et al. [15-20, 33-39]. Peaks at 19.5 eV and 36.0 eV which do not correspond to any other primary element peaks were observed. The

relative intensities and shift of each peak match $K\,3s$ and $K\,3p$ peaks shifted to higher binding energies. Hydrogen is the only element which does not have primary element peaks; thus, it is the only candidate to produce the shifted peaks. These peaks may be shifted by a highly binding hydride ion with a binding energy of 22.8 eV [15-20, 33-39] that bonds to potassium $K\,3p$ and shifts the peak to this energy. In this case, the $K\,3s$ is similarly shifted. The shift of about 3 eV is greater than that of known potassium compounds. These peaks were not present in the case of the XPS of matching samples isolated from an identical electrolytic cell except that Na_2CO_3 replaced K_2CO_3 as the electrolyte.

The KH electrolytic cell sample was observed to be weakly ferromagnetic. The origin of the magnetism is from nonmetallic elements which were most likely potassium and hydrogen.

3.3. NMR

The signal intensities of the ^1H MAS NMR spectrum of the K_2CO_3 reference were relatively low. It contained a water peak at 1.208 ppm, a peak at 5.604 ppm, and very broad weak peaks at 13.2 ppm, and 16.3 ppm. The ^1H MAS NMR spectrum of the $KHCO_3$ reference contained a large peak at 4.745 with a small shoulder at 5.150 ppm, a broad peak at 13.203 ppm, and small peak at 1.2 ppm.

The ^1H MAS NMR spectra of the $KH\,KHCO_3$ electrolytic cell sample is shown in Fig. 14. The peak assignments are given in Table III. The reproducible peaks assigned to $KH\,KHCO_3$ in Table III were not present in the controls except for the peak assigned to water at +5.066 ppm. The novel peaks could not be assigned to hydrocarbons. Hydrocarbons were not present in the electrolytic cell sample based on the ToF-SIMS spectrum and FTIR spectra which were also obtained (see below). The novel peaks without identifying assignment are consistent with $KH\,KHCO_3$. The NMR peaks of the reference KH (Aldrich Chemical Company 99%) were observed at 0.8 and 1.1 ppm relative to TMS. The upfield peaks of Fig. 14 are assigned to novel hydride ion of the potassium hydride species ($KH-$) in different environments. The down field peaks are assigned to the proton of the potassium hydrogen carbonate species in different chemical environments ($-KHCO_3$).

3.4. FTIR

The FTIR spectra of K_2CO_3 (99%) and $KHCO_3$ (99.99%) were compared with that of the $KH\,KHCO_3$ electrolytic cell sample. A spectrum of a mixture of the bicarbonate and the carbonate was produced by digitally adding the two reference spectra. The two standards alone

and the mixed standards were compared with that of the electrolytic cell sample. From the comparison, it was determined that the electrolytic cell sample contained potassium carbonate but did not contain potassium bicarbonate. The unknown component could be a bicarbonate other than potassium bicarbonate. The spectrum of potassium carbonate was digitally subtracted from the spectrum of the electrolytic cell sample as shown in Fig. 15. Several bands were observed including bands in the $1400-1600\ cm^{-1}$ region. Some organic nitrogen compounds (e.g. acrylamides, pyrolidinones) have strong bands in the region $1660\ cm^{-1}$ [48]. However, the lack of any detectable $C-H$ bands ($\approx 2800-3000\ cm^{-1}$) and the bands present in the 700 to 1100 cm^{-1} region indicate an inorganic material [49]. Peaks that are not assignable to potassium carbonate were observed at 3294, 3077, 2883, 1100 cm^{-1}, 2450, 1660, 1500, 1456, 1423, 1300, 1154, 1023, 846, 761, and 669 cm^{-1}.

The overlap FTIR spectrum of the electrolytic cell sample and the FTIR spectrum of the reference potassium carbonate appears in Fig. 16. In the 700 to 2500 cm^{-1} region, the peaks of the electrolytic cell sample closely resemble those of potassium carbonate, but they are shifted about 50 cm^{-1} to lower frequencies. The shifts are similar to those observed by replacing potassium (K_2CO_3) with rubidium (Rb_2CO_3) as demonstrated by comparing their IR spectra [50]. The shifted peaks may be explained by a polymeric structure for the compound $KH\,KHCO_3$ wherein the vibrational frequency is inversely proportional to the square root of the mass. The polymeric structure is supported by the observation of multimers of $140n$ in the positive ToF-SIMS spectrum of the electrolytic cell sample.

3.5. Mass Spectroscopy (MS)

The KH electrolytic cell sample did not decompose upon heating to 600°C. Essentially no hydrogen was observed by mass spectroscopy. The sample changed very little which indicates no decomposition and extraordinary stability for a compound mainly comprised of hydrogen.

3.6. Further Analytical Tests

X-ray diffraction (XRD), elemental analysis, and Raman spectroscopy were also performed on the $KH\,KHCO_3$ electrolytic sample. The XRD data indicated that the diffraction pattern of the electrolytic cell sample does not match that of either KH, $KHCO_3$, K_2CO_3, or KOH. The elemental analysis (Galbraith Laboratories) showed a wt % of potassium, carbon, and hydrogen of 43.65, 7.91, and 1.43, respectively. Oxygen could not be obtained. The corresponding high hydrogen atomic percentage supports $KH\,KHCO_3$. Unidentified Raman

peaks at 1685 cm^{-1} and 835 cm^{-1} were present in addition to the known peaks of $KHCO_3$ and a small peak assignable to K_2CO_3.

Results from gaseous reactions at elevated temperature demonstrate that $KH\,KHCO_3$ may also be formed by a reaction of gaseous KI with atomic hydrogen in the presence of K_2CO_3 [37]. In addition to the previous analytical studies, the fragment $KK_2CO_3^+$ corresponding to $KH\,KHCO_3$ was observed by ESIToFMS as a chromatographic peak on a C18 liquid chromatography column typically used to separate organic compounds. No chromatographic peaks were observed in the case of inorganic compound controls KI, $KHCO_3$, K_2CO_3, and KOH.

3.7. Insitu High Resolution Visible Spectroscopy

The low resolution spectrum of each electrolysis plasma was recorded over the range 400 – 900 *nm* to identify emitting species such as hydrogen and alkali species as demonstrated by the low resolution spectrum of the K_2CO_3 electrolysis plasma shown in Fig. 17. In each case, strong alkali metal, Balmer α, and molecular hydrogen emission was observed. In addition, weaker alkali metal ion emission was observed for each plasma except for the Na_2CO_3 plasma. The alkali emission lines are given in Table IV.

The high resolution visible spectrum in the region of 407 nm was recorded on the emission from each of the plasma electrolysis cells. A peak at 407.0 nm was observed in each case except for the Na_2CO_3 cell. To eliminate tungsten emission as the source of the 407.0 nm peak, each plasma electrolysis was repeated with a platinum cathode.

The high resolution visible spectra in the region of 407 nm from the Na_2CO_3, K_2CO_3, Rb_2CO_3, and Cs_2CO_3 plasma electrolysis cells each with a platinum cathode are shown in Figs. 18–21, respectively. The only peaks observed from the Na_2CO_3 plasma were known peaks of molecular hydrogen; whereas, in each case of the K_2CO_3, Rb_2CO_3, and Cs_2CO_3 plasma, a peak was observed at 407.0 nm which could not be assigned to hydrogen, the alkali or alkaline earth atom or ion, or platinum. The known peaks of molecular hydrogen in the region of 407 nm were separated as indicated in Figs. 18–21.

Since the novel 407.0 nm peak was also only observed for the K_2CO_3, Rb_2CO_3, and Cs_2CO_3 plasma electrolysis cells, but not for the Na_2CO_3 cell when the tungsten cathode was replaced by a platinum cathode, cathode metal lines were eliminated as the source of the novel 407.0 nm peak. O II lines at 406.9623, 406.9881, and 407.1238 nm were also eliminated due to the absence of O I lines at 394.729, 394.748, 394.758, 395.460, and 405.477 nm. C III lines at 407.026 and 406.8916 nm were eliminated due to the absence of C I lines which were outside of the region of 407.0 nm or C II lines at 391.896 and 392.068 nm. Furthermore, the

presence of the O II or C III lines would be extraordinary since the ionization energy required for O II is above the first ionization energy of 13.62 eV, and the energies required for C III are above the sum of the first and second ionization energies of 11.26 eV and 24.38 eV, respectively [43].

4. DISCUSSION

Alkali and alkaline earth hydrides react violently with water to release hydrogen gas which subsequently ignites due to the exothermic reaction with water. Typically metal hydrides decompose upon heating at a temperature in the range of 250-1000°C. These saline hydrides, so called because of their saltlike or ionic character, are the monohydrides of the alkali metals and the dihydrides of the alkaline-earth metals, with the exception of beryllium. BeH_2 appears to be a hydride with bridge type bonding rather than an ionic hydride. Highly polymerized molecules held together by hydrogen-bridge bonding is exhibited by boron hydrides and aluminum hydride. Based on the known structures of these hydrides, the ToF-SIMS hydride clusters such as $K[KH\,KHCO_3]_n^+$, the XPS peaks observed at 22.8 eV and 38.8 eV, upfield NMR peaks assigned to hydride ion, and the shifted FTIR peaks, the present novel hydride compound of the $KH\,KHCO_3$ electrolytic cell sample may be a polymer, $[KH\,KHCO_3]_n$, with a structural formula which is similar to boron and aluminum hydrides. The reported novel compound appeared polymeric in the concentrated electrolytic solution and in distilled water. $[KH\,KHCO_3]_n$ is extraordinarily stable in water; whereas, potassium hydride reacts violently with water.

As an example of the structures of this compound, the $K[KH\,KHCO_3]_n^+$ $m/z = (39 + 140n)$ series of fragment peaks is tentatively assigned to novel hydride bridged or linear potassium bicarbonate compounds having a general formula such as $[KHKHCO_3]_n$ $n = 1,2,3....$ General structural formulas may be

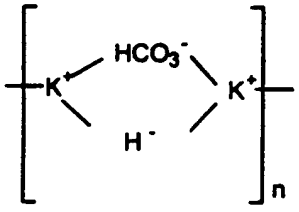

and

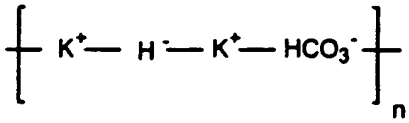

Liquid chromatography/ESIToFMS studies are in progress to support the polymer assignment.

KH was stable at elevated temperature (600°C). The positive and negative ToF-SIMS of the KH electrolytic sample showed essentially K^+ and H^- only, respectively. Hydride ions with binding energies of 22.8 eV and 69.2 eV have been observed by XPS of KH. The former hydride ion with a binding energy of 22.8 eV was observed by X-ray photoelectron spectroscopy (XPS) of the $KH\,KHCO_3$ electrolytic sample. These compounds appear polymeric in aqueous solution. KH was observed to be weakly ferromagnetic; whereas, $KH\,KHCO_3$ was diamagnetic. The magnetism of KH may be due to mixed oxidation states due to the presence of two hydride ions with a substantially reduced radii to permit spin correlation.

Each of K^+ / K^+, Rb^+, and Cs as the catalyst was predicted to catalyze hydrogen to form $H\left[\frac{a_H}{2}\right]$ which reacts with an electron to form $H^-(1/2)$. The predicted $H^-(1/2)$ hydride ion of hydrogen catalysis by these catalysts was observed spectroscopically at 407.0 nm corresponding to its predicted binding energy of 3.05 eV. The hydride reaction product formed over time and was stable in water. The formation of hydride novel compounds observed by ToF-SIMS provided substantial evidence supporting catalysis of hydrogen to form $H^-(1/2)$ and its spectroscopic identification.

5. CONCLUSION

The ToF-SIMS, XPS, and NMR results of products from a K_2CO_3 electrolytic cell with K^+ / K^+ as the catalyst confirm the identification of $KH\,KHCO_3$ and KH with new states of hydride ions. $H^-(1/2)$, the predicted hydride ion product with each of K^+ / K^+, Rb^+, and Cs as the catalyst, has a binding energy of 3.05 eV corresponding to a 407 nm emission. Metal and/or metal ion peaks corresponding to the electrolyte (K, Rb, Cs, Na), molecular hydrogen, and atomic hydrogen were observed by high resolution visible spectroscopy in plasma electrolysis cells. The $H^-(1/2)$ peak at 407.0 nm was observed in all of the electrolytes except Na_2CO_3 which cannot form $H^-(1/2)$. It was remarkable that the hydride ion formed in aqueous solution which is indicative of its stability and potential novel chemistry.

The chemical structure and properties of the novel compounds having hydride ions with high binding energies are indicative of a new field of hydride chemistry. The novel hydride ions may combine with other cations such as other alkali cations and alkaline earth, rare earth, and transition element cations. Thousands of novel compounds may be synthesized with extraordinary properties relative to the corresponding compounds having ordinary hydride ions. These novel compounds may have a breadth of applications. For example, a high voltage battery (eqs. (1)–(3)) according to the hydride binding energies of 22.8 eV and

69.2 *eV* observed by XPS may be possible having projected specifications and environmental advantages that may be competitive with the internal combustion engine.

ACKNOWLEDGMENTS

Special thanks to F. Becker for assistance with the power electronics and monitoring systems.

REFERENCES

1) I. Uehara, T. Sakai, H. Ishikawa: J. Alloy Comp. **253/254** (1997) No. 1/2, 635.

2) J. Glanz: New Scientist. **146** (1995) No. 1973, 32.

3) D. Mulholland: Defense News. **14** (1999) No. 10, 1 and 34.

4) S. M. Aceves, G. D. Berry, and G. D. Rambach: Int. J. Hydrogen Energy. **23** (1998) No. 7, 583.

5) J. Ball: Auto Makers Are Racing to Market "Green" Cars Powered by Fuel Cells published in The Wall Street Journal. March 15, (1999) p. 1.

6) US Office of Technology Assessment: *Advanced Automotive Technology: Visions of a Super-Efficient Family Car*, National Technical Information Service, US Department of Commerce, PB96-109202, OTA-ETI-638 (1995).

7) R. Mills: *The Grand Unified Theory of Classical Quantum Mechanics* (BlackLight Power, Inc.: Cranbury, New Jersey, 2000, Distributed by Amazon.com; September 2001 Edition posted at www.blacklightpower.com.)

8) R. Mills: *Proc.* 29th *Conference on High Energy Physics and Cosmology, 2000* (Kluwer Academic/Plenum Publishers, New York, 2001) p. 243.

9) R. Mills: The Grand Unified Theory of Classical Quantum Mechanics to be published in Int. J. of Hydrogen Energy. (2002).

10) R. Mills: Int. J. of Hydrogen Energy. **25** (2000) 1171.

11) R. Mills: Int. J. Hydrogen Energy **26** (2001) 1059.

12) R. Mills and P. Ray: Spectral Emission of Fractional Quantum Energy Levels of Atomic Hydrogen from a Helium-Hydrogen Plasma and the Implications for Dark Matter to be published in Int. J. Hydrogen Energy. (2002).

13) R. L. Mills, P. Ray, B. Dhandapani and J. He: Spectroscopic Identification of Fractional Rydberg States of Atomic Hydrogen submitted to J. Phys. Chem. Letts.

14) R. Mills and P. Ray: Vibrational Spectral Emission of Fractional-Principal-Quantum-Energy-Level Hydrogen Molecular Ion to be published in Int. J. Hydrogen Energy. (2002).

15) R. Mills, P. Ray, M. Nansteel, W. Good, P. Jansson, B. Dhandapani and J. He: Excessive Balmer α Line Broadening, Power Balance, and Novel Hydride Ion Product of Plasma Formed from Incandescently Heated Hydrogen Gas with Certain Catalysts submitted to Int. J. Hydrogen Energy.

16) R. L. Mills and P. Ray: High Resolution Spectroscopic Observation of the Bound-Free Hyperfine Levels of a Novel Hydride Ion Corresponding to a Fractional Rydberg State of Atomic Hydrogen submitted to Int. J. Hydrogen Energy.

17) R. L. Mills and E. Dayalan: *Proc. 17th Annual Battery Conference on Applications and Advances, 2002,* (California State University, Long Beach, 2002.)

18) R. L. Mills and P. Ray: Spectroscopic Identification of a Novel Catalytic Reaction of Rubidium Ion with Atomic Hydrogen and the Hydride Ion Product submitted to Int. J. Hydrogen Energy.

19) R. Mills and P. Ray: Int. J. Hydrogen Energy. **27** (2002) 183.

20) R. Mills: Int. J. Hydrogen Energy. **26** (2001) 1041.

21) R. Mills and M. Nansteel: Argon-Hydrogen-Strontium Plasma Light Source submitted to IEEE Transactions on Plasma Science.

22) R. Mills, M. Nansteel, and P. Ray: Excessively Bright Hydrogen-Strontium Plasma Light Source Due to Energy Resonance of Strontium with Hydrogen submitted to European Journal of Physics D.

23) R. Mills, J. Dong, W. Good, P. Ray, J. He, and B. Dhandapani: Measurement of Energy Balances of Noble Gas-Hydrogen Discharge Plasmas Using Calvet Calorimetry submitted to Int. J. Hydrogen Energy.

24) Randell L. Mills, P. Ray, B. Dhandapani, M. Nansteel, X. Chen and J. He: New Power Source from Fractional Quantum Energy Levels of Atomic Hydrogen that Surpasses Internal Combustion submitted to Spectrochimica Acta Part A.

25) R. L. Mills, P. Ray, B. Dhandapani and J. He: Comparison of Excessive Balmer α Line Broadening of Glow Discharge and Microwave Hydrogen Plasmas with Certain Catalysts submitted to J. Phys. Chem.

26) R. L. Mills, A. Voigt, P. Ray, M. Nansteel and B. Dhandapani: Measurement of Hydrogen Balmer Line Broadening and Thermal Power Balances of Noble Gas-Hydrogen Discharge Plasmas to be published in Int. J. Hydrogen Energy. (2002).

27) R. Mills, N. Greenig and S. Hicks: Optically Measured Power Balances of Anomalous Discharges of Mixtures of Argon, Hydrogen, and Potassium, Rubidium, Cesium, or Strontium Vapor to be published in Int. J. Hydrogen Energy. (2002).

28) R. Mills, M. Nansteel, and Y. Lu: Int. J. Hydrogen Energy. **26** (2001) 309.

29) R. Mills, J. Dong and Y. Lu: Int. J. Hydrogen Energy. **25** (2000) 919.

30) R. Mills: Int. J. Hydrogen Energy. **26** (2001) 579.

31) R. Mills: Int. J. Hydrogen Energy, **26** (2001) 327.

32) R. Mills, T. Onuma, and Y. Lu: Int. J. Hydrogen Energy. **26** (2001) 749.

33) R. Mills, B. Dhandapani, M. Nansteel, J. He and A. Voigt: Int. J. Hydrogen Energy. **26** (2001) 965.

34) R. Mills, B. Dhandapani, N. Greenig and J. He: Int. J. of Hydrogen Energy. **25** (2000) 1185.

35) R. Mills: Int. J. of Hydrogen Energy. **25** (2000) 669.
36) R. Mills: Fusion Technology. **37** (2000) No. 2, 157.
37) R. Mills, B. Dhandapani, M. Nansteel, J. He, T. Shannon and A. Echezuria: Int. J. of Hydrogen Energy. **26** (2001) 339.
38) R. Mills: Highly Stable Novel Inorganic Hydrides to be published in Journal of New Materials for Electrochemical Systems. (2002).
39) R. Mills, W. Good, A. Voigt, J. Dong: **26** (2001) 1199.
40) R. Mills: *Proc. National Hydrogen Association, 12th Annual U.S. Hydrogen Meeting and Exposition, Hydrogen: The Common Thread, 2001.* (National Hydrogen Association, Washington, DC, 2001) p. 671.
41) R. Mills: *Proceedings of Global Foundation International Conference on Global Warming and Energy Policy, 2001.* (Kluwer Academic/Plenum Publishers, New York) p. 1059.
42) R. Mayo, R. Mills and M. Nansteel: On the Potential of Direct and MHD Conversion of Power from a Novel Plasma Source to Electricity for Microdistributed Power Applications submitted to IEEE Transactions on Plasma Science.
43) David R. Linde, *CRC Handbook of Chemistry and Physics*, 79 th Edition, CRC Press, Boca Raton, Florida, (1998-9), p. 10-175–10-177.
44) Microsc. Microanal. Microstruct. **3** (1992) No. 1.
45) For recent specifications see PHI Trift II, ToF-SIMS Technical Brochure, (1999), Eden Prairie, MN 55344.
46) D. Briggs, M. P. Seah, eds.: *Practical Surface Analysis, 2E., Vol. 2, Ion and Neutral Spectroscopy.* (Wiley & Sons, New York, 1992).
47) C. D. Wagner, W. M. Riggs, L. E. Davis, J. F. Moulder: *Handbook of X-ray Photoelectron Spectroscopy*, ed: G. E. Mullenberg (Perkin-Elmer Corp., Eden Prairie, Minnesota, 1997).
48) D. Lin-Vien, N. B. Colthup, W. G. Fateley and J. G. Grasselley: *The Handbook of Infrared and Raman Characteristic Frequencies of Organic Molecules* (Academic Press, Inc., San Diego, CA, 1991).
49) R. A. Nyquist and R. O. Kagel, eds.: *Infrared Spectra of Inorganic Compounds* (Academic Press, New York, 1971).
50) M. H. Brooker and J. B. Bates: Spectrochimica Acta Part A—Molecular and Biomolecular Spectroscopy. **A 30** (1974) 2211.

Figure Captions

Figure 1. Plasma electrolysis cell for synthesis of novel hydride compounds and as a source of light from the cathodic plasma for high resolution visible spectroscopy.

Figure 2. The positive ToF-SIMS spectrum ($m/e = 0 - 200$) of $KHCO_3$ (99.99%) where HC = hydrocarbon.

Figure 3. The positive ToF-SIMS spectrum ($m/e = 200 - 1000$) of $KHCO_3$ (99.99%) where HC = hydrocarbon.

Figure 4. The positive ToF-SIMS spectrum ($m/e = 0 - 200$) of the $KH\,KHCO_3$ electrolytic cell sample where HC = hydrocarbon.

Figure 5. The positive ToF-SIMS spectrum ($m/e = 200 - 1000$) of the $KH\,KHCO_3$ electrolytic cell sample where HC = hydrocarbon.

Figure 6. The negative ToF-SIMS spectrum ($m/e = 0 - 50$) of the $KHCO_3$ (99.99%) sample.

Figure 7. The negative ToF-SIMS spectrum ($m/e = 0 - 30$) of the $KH\,KHCO_3$ electrolytic cell sample.

Figure 8. The positive ToF-SIMS spectrum ($m/e = 0 - 400$) of the KH electrolytic cell sample.

Figure 9. The negative ToF-SIMS spectrum ($m/e = 0 - 400$) of the KH electrolytic cell sample.

Figure 10. The 0 to 80 eV binding energy region of a high resolution XPS spectrum of the $KH\,KHCO_3$ electrolytic cell sample.

Figure 11. The XPS survey spectrum of the $KH\,KHCO_3$ electrolytic cell sample with the primary elements identified.

Figure 12. The XPS survey scan of the KH electrolytic cell sample.

Figure 13. The 0-80 eV binding energy region of a high resolution XPS spectrum of the KH electrolytic cell sample.

Figure 14. The magic angle spinning proton NMR spectrum of the $KH\,KHCO_3$ electrolytic cell sample.

Figure 15. The spectrum of potassium carbonate digitally subtracted from the spectrum of the electrolytic cell sample.

Figure 16. The overlap FTIR spectrum of the $KH\,KHCO_3$ electrolytic cell sample and the FTIR spectrum of the reference potassium carbonate.

Figure 17. The low resolution spectrum ($400 - 800\ nm$) of the K_2CO_3 electrolysis plasma cell showing the emission from atomic hydrogen, molecular hydrogen, potassium metal, and K^+.

Figure 18. The high resolution visible spectrum in the region of 407 nm recorded on the emission of Na_2CO_3 plasma electrolysis cell with a platinum cathode. All of the peaks could be assigned to known lines of molecular hydrogen.

Figure 19. The high resolution visible spectrum in the region of 407 nm recorded on the emission of K_2CO_3 plasma electrolysis cell with a platinum cathode. The novel 407.0 nm peak which could not be assigned to a known peak was assigned to $H^-(1/2)$.

Figure 20. The high resolution visible spectrum in the region of 407 nm recorded on the emission of Rb_2CO_3 plasma electrolysis cell with a platinum cathode. The novel 407.0 nm peak which could not be assigned to a known peak was assigned to $H^-(1/2)$.

Figure 21. The high resolution visible spectrum in the region of 407 nm recorded on the emission of Cs_2CO_3 plasma electrolysis cell with a platinum cathode. The novel 407.0 nm peak which could not be assigned to a known peak was assigned to $H^-(1/2)$.

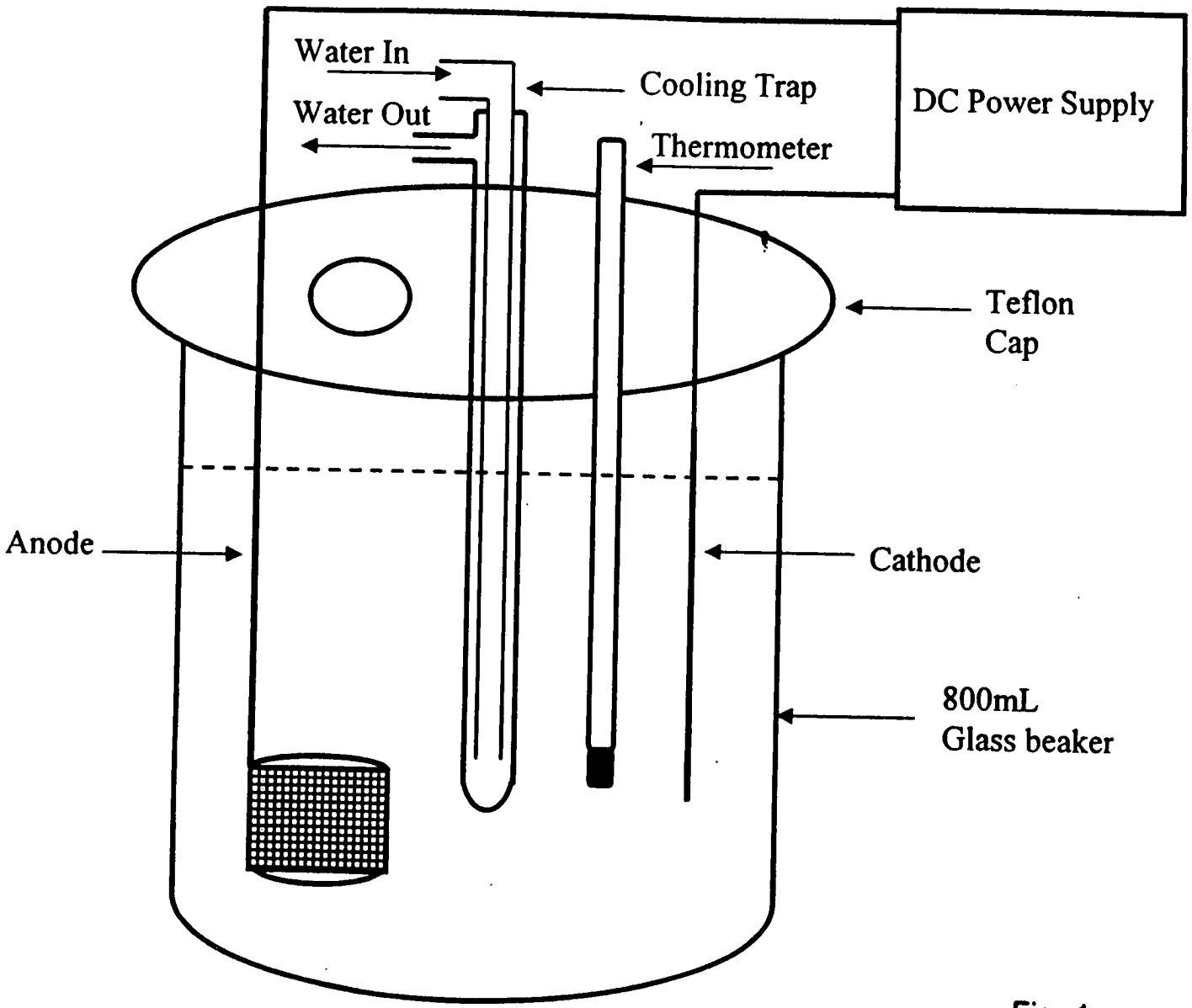
Water In
Water Out
Cooling Trap
Thermometer
DC Power Supply
Teflon
Cap
Anode
Cathode
800mL
Glass beaker

Fig. 1

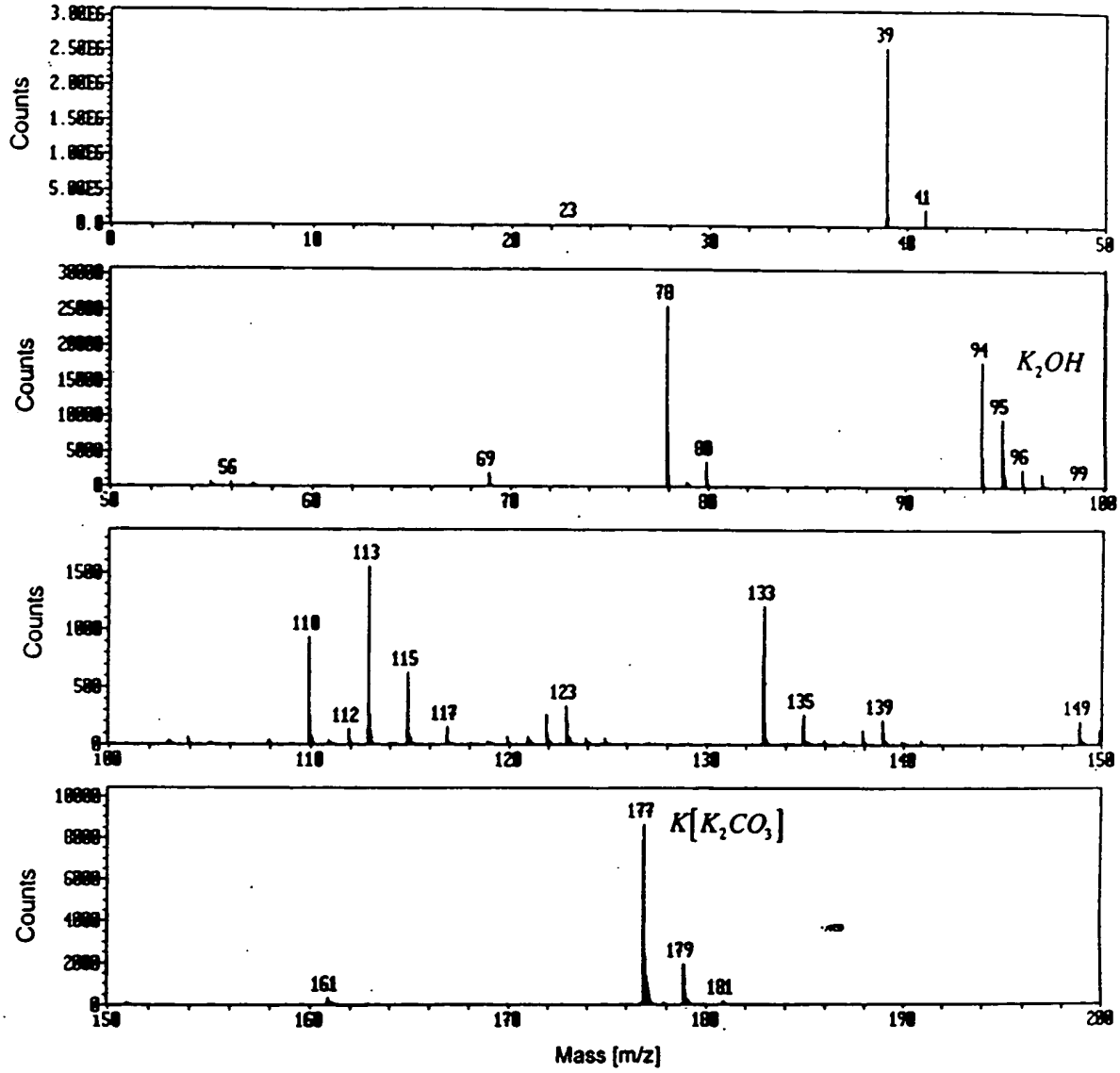
Counts
39
23
41
78
94
K_2OH
95
56
69
88
96
99
113
118
133
115
112
117
123
135
139
149
177
$K[K_2CO_3]$
179
161
181
Mass [m/z]

Fig. 2

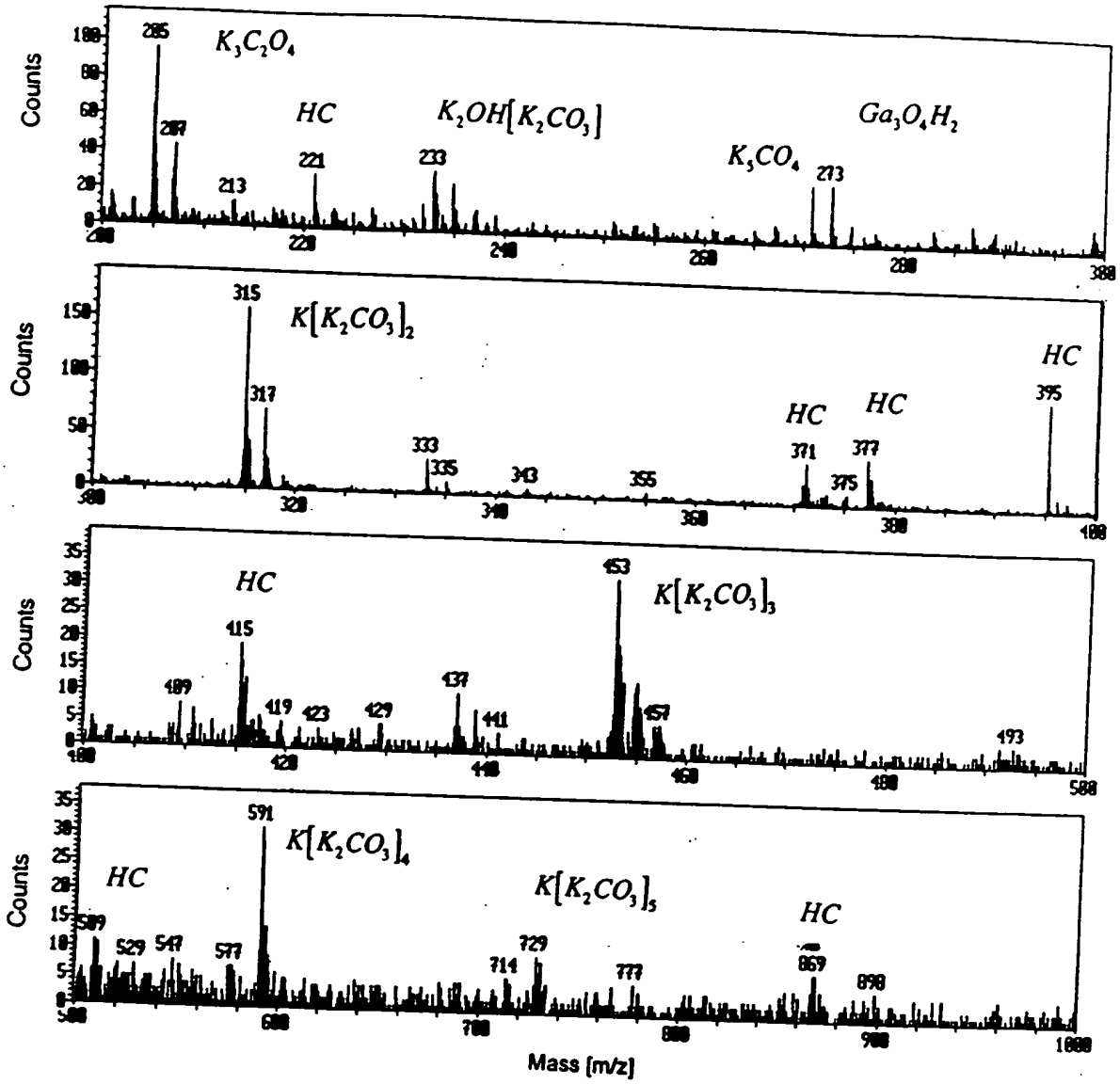
Counts
285
$K_3C_2O_4$
287
213
HC
221
$K_2OH[K_2CO_3]$
233
K_5CO_4
273
$Ga_3O_4H_2$
315
$K[K_2CO_3]_2$
317
333
335
343
355
HC
371
HC
377
375
HC
395
453
$K[K_2CO_3]_3$
HC
415
389
419
423
429
437
441
457
493
591
$K[K_2CO_3]_4$
HC
589
529
547
577
$K[K_2CO_3]_5$
729
714
777
HC
869
898
Mass [m/z]

Fig. 3

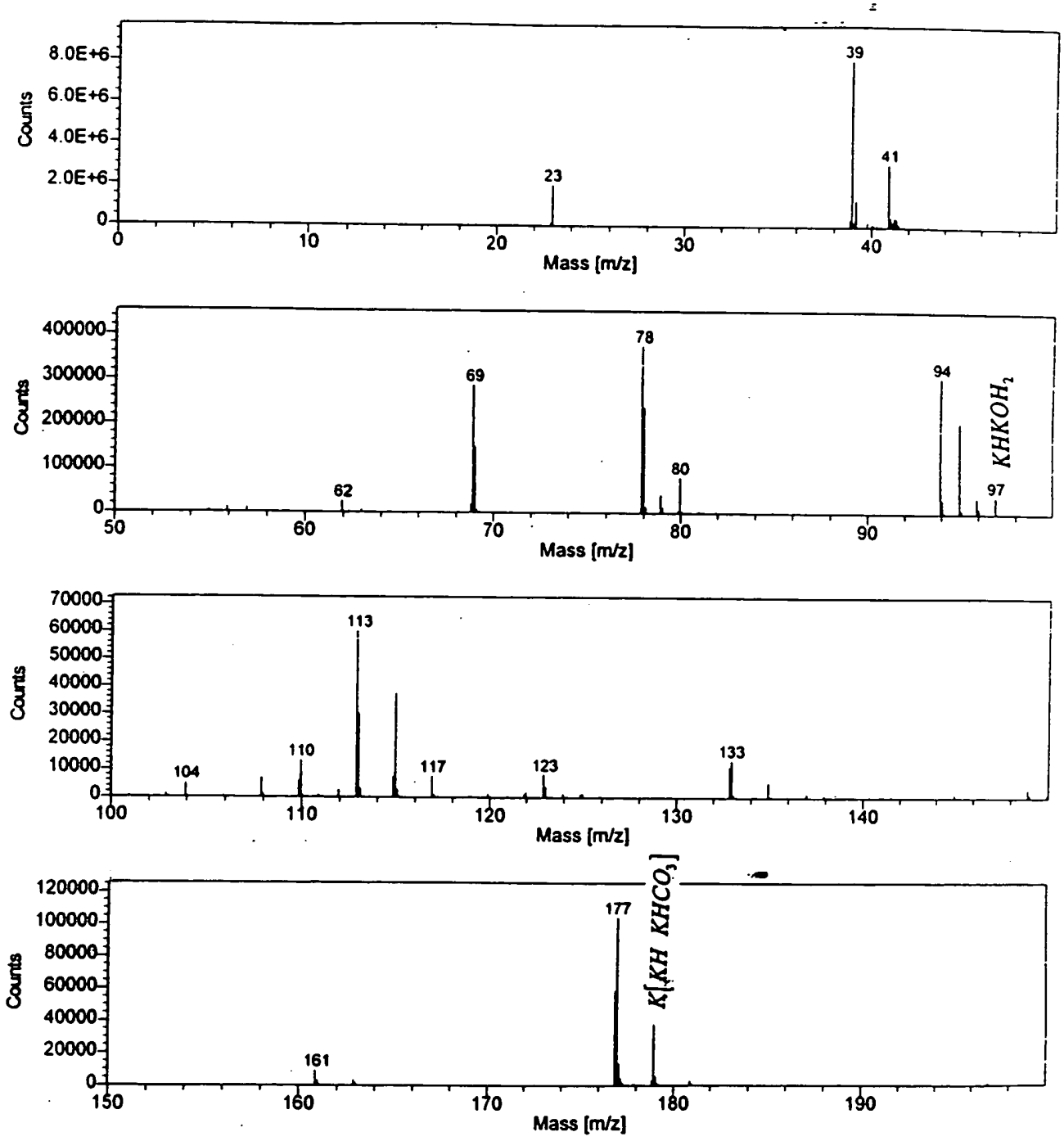
Counts
8.0E+6
6.0E+6
4.0E+6
2.0E+6
0
39
41
23
0
10
20
30
40
Mass [m/z]
400000
300000
200000
100000
0
78
69
94
80
62
97
$KHKOH_2$
50
60
70
80
90
Mass [m/z]
70000
60000
50000
40000
30000
20000
10000
0
113
110
104
117
123
133
100
110
120
130
140
Mass [m/z]
120000
100000
80000
60000
40000
20000
0
177
$K[KH\ KHCO_3]$
161
150
160
170
180
190
Mass [m/z]

Fig. 4

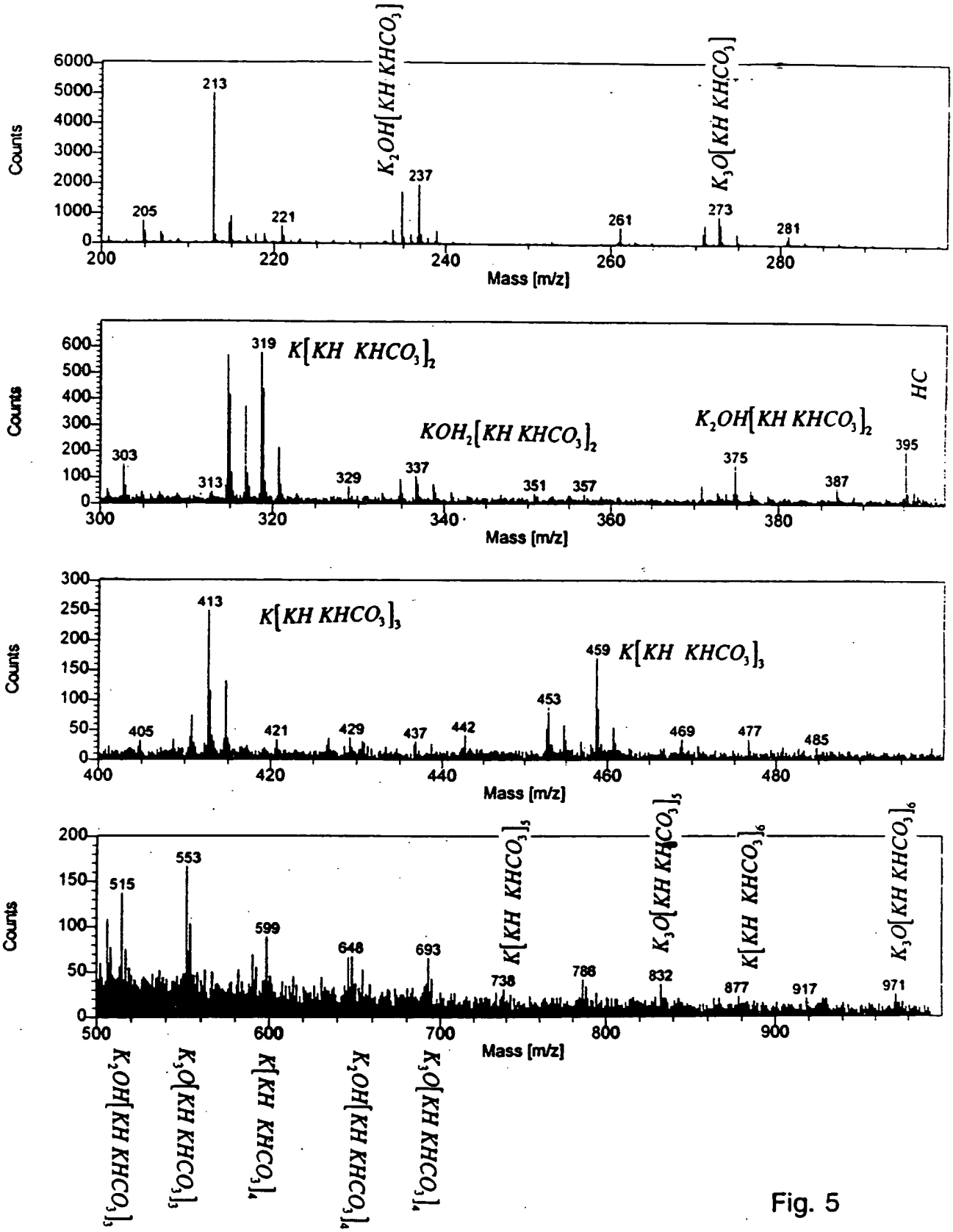
Counts
Mass [m/z]
213
205
221
237
261
273
281
$K_2OH[KH\ KHCO_3]$
$K_3O[KH\ KHCO_3]$
319
303
313
329
337
351
357
375
387
395
$K[KH\ KHCO_3]_2$
$KOH_2[KH\ KHCO_3]_2$
$K_2OH[KH\ KHCO_3]_2$
HC
413
405
421
429
437
442
453
459
469
477
485
$K[KH\ KHCO_3]_3$
$K[KH\ KHCO_3]_3$
515
553
599
648
693
738
788
832
877
917
971
$K[KH\ KHCO_3]_5$
$K_3O[KH\ KHCO_3]_5$
$K[KH\ KHCO_3]_6$
$K_3O[KH\ KHCO_3]_6$
$K_2OH[KH\ KHCO_3]_3$
$K_3O[KH\ KHCO_3]_3$
$K[KH\ KHCO_3]_4$
$K_2OH[KH\ KHCO_3]_4$
$K_3O[KH\ KHCO_3]_4$

Fig. 5

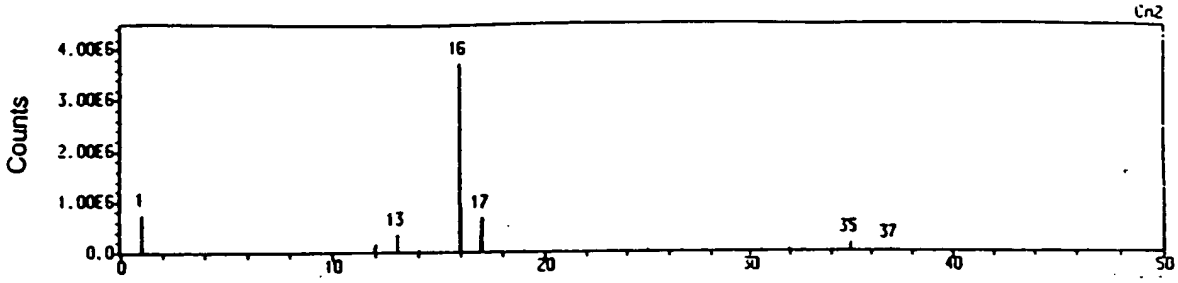
Cn2
Counts
4.00E6
3.00E6
2.00E6
1.00E6
0.0
1
13
16
17
35
37
0
10
20
30
40
50

Fig. 6

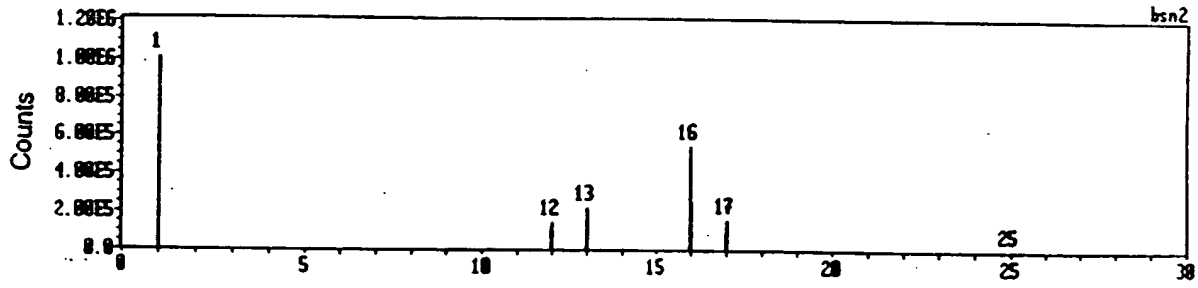
bsn2
Counts
1.20E6
1.00E6
8.00E5
6.00E5
4.00E5
2.00E5
0.0
0
5
10
15
20
25
30
1
12
13
16
17
25

Fig. 7

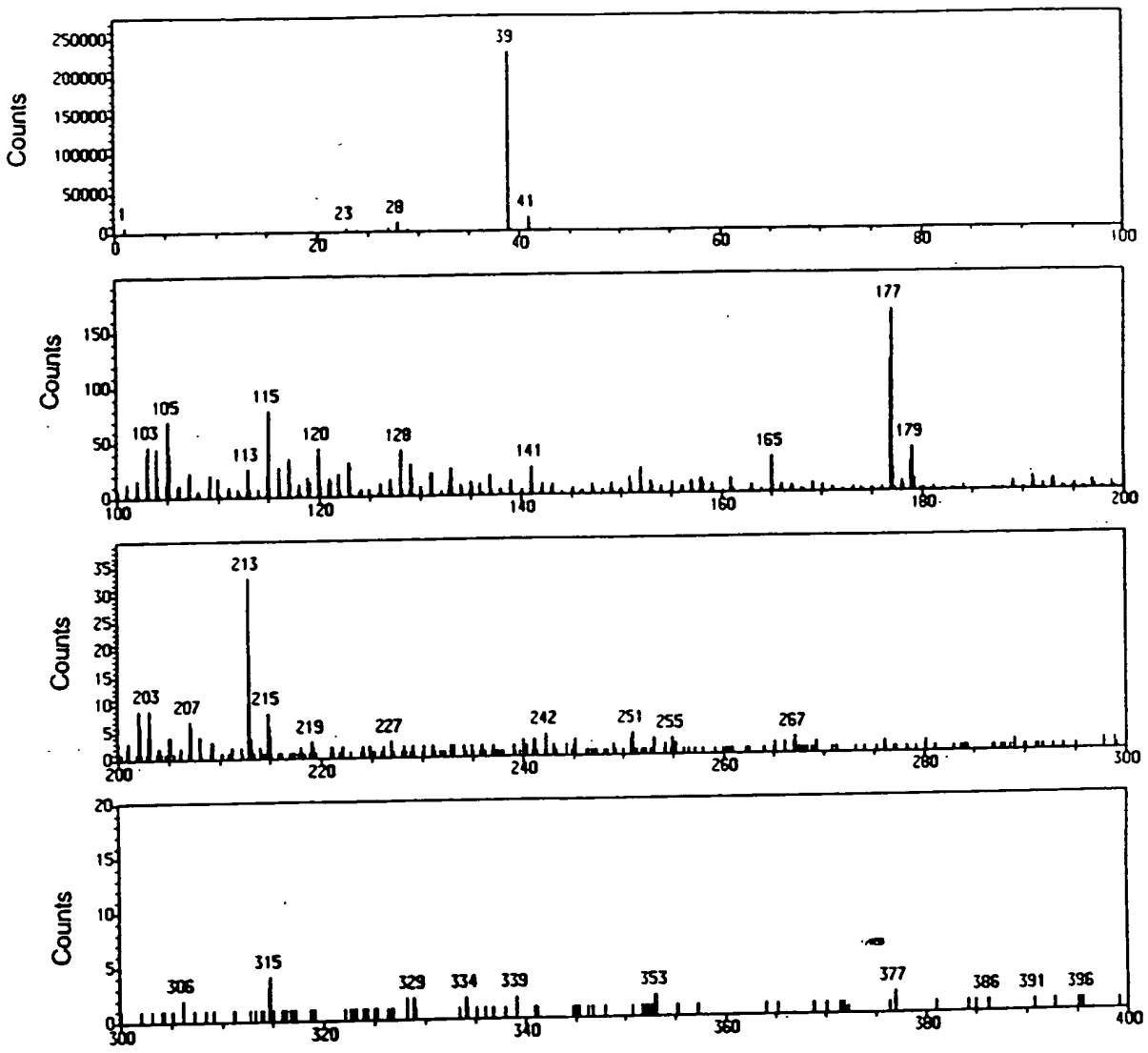
Counts
39
23
28
41
1
Counts
177
105
115
103
113
120
128
141
165
179
Counts
213
203
207
215
219
227
242
251
255
267
Counts
315
306
329
334
339
353
377
386
391
396

Fig. 8

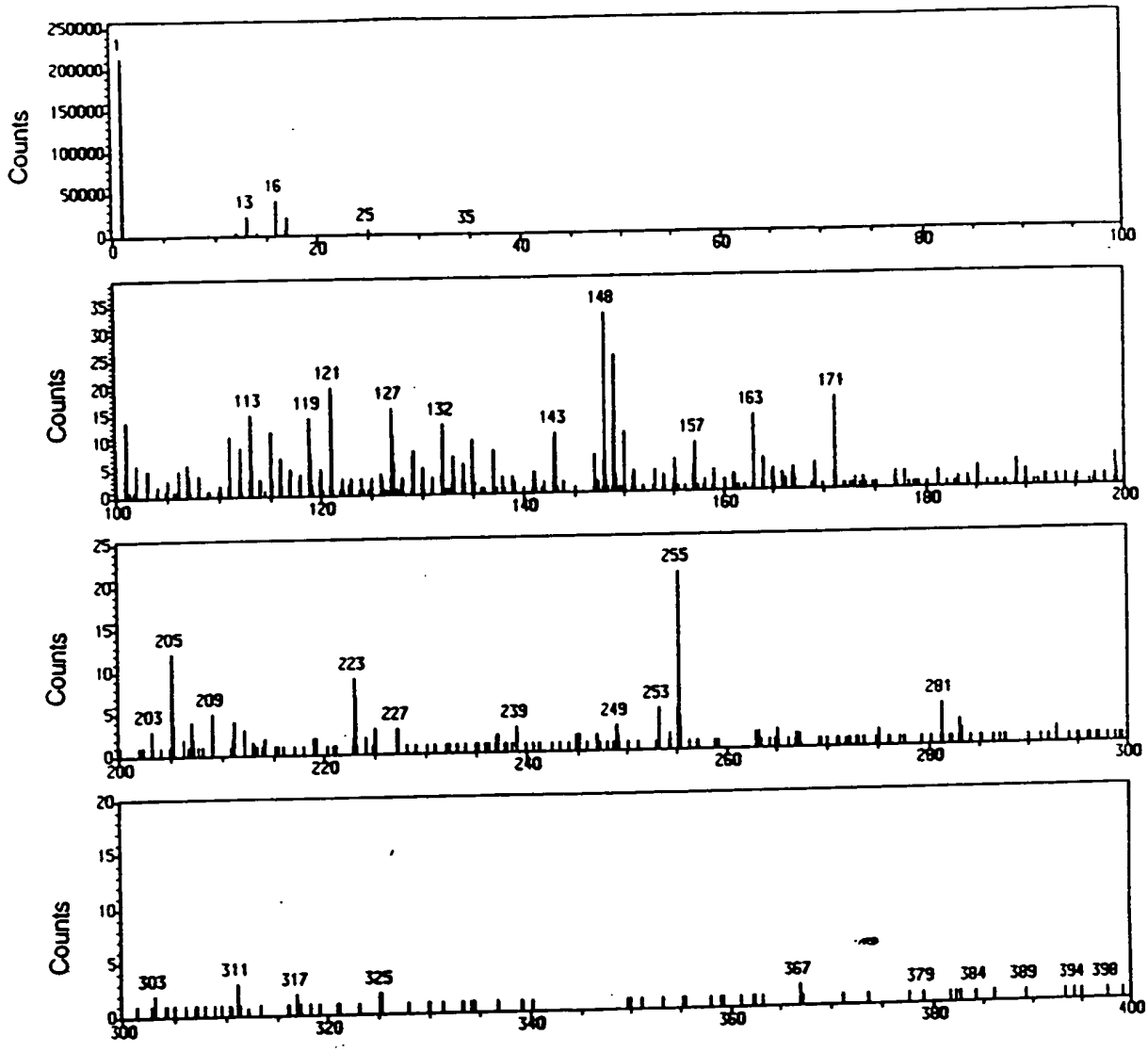
Counts
250000
200000
150000
100000
50000
0
1
13
16
25
35
0
20
40
60
80
100
Counts
35
30
25
20
15
10
5
0
113
119
121
127
132
143
148
157
163
171
100
120
140
160
180
200
Counts
25
20
15
10
5
0
203
205
209
223
227
239
249
253
255
281
200
220
240
260
280
300
Counts
20
15
10
5
0
303
311
317
325
367
379
384
389
394
398
300
320
340
360
380
400

Fig. 9

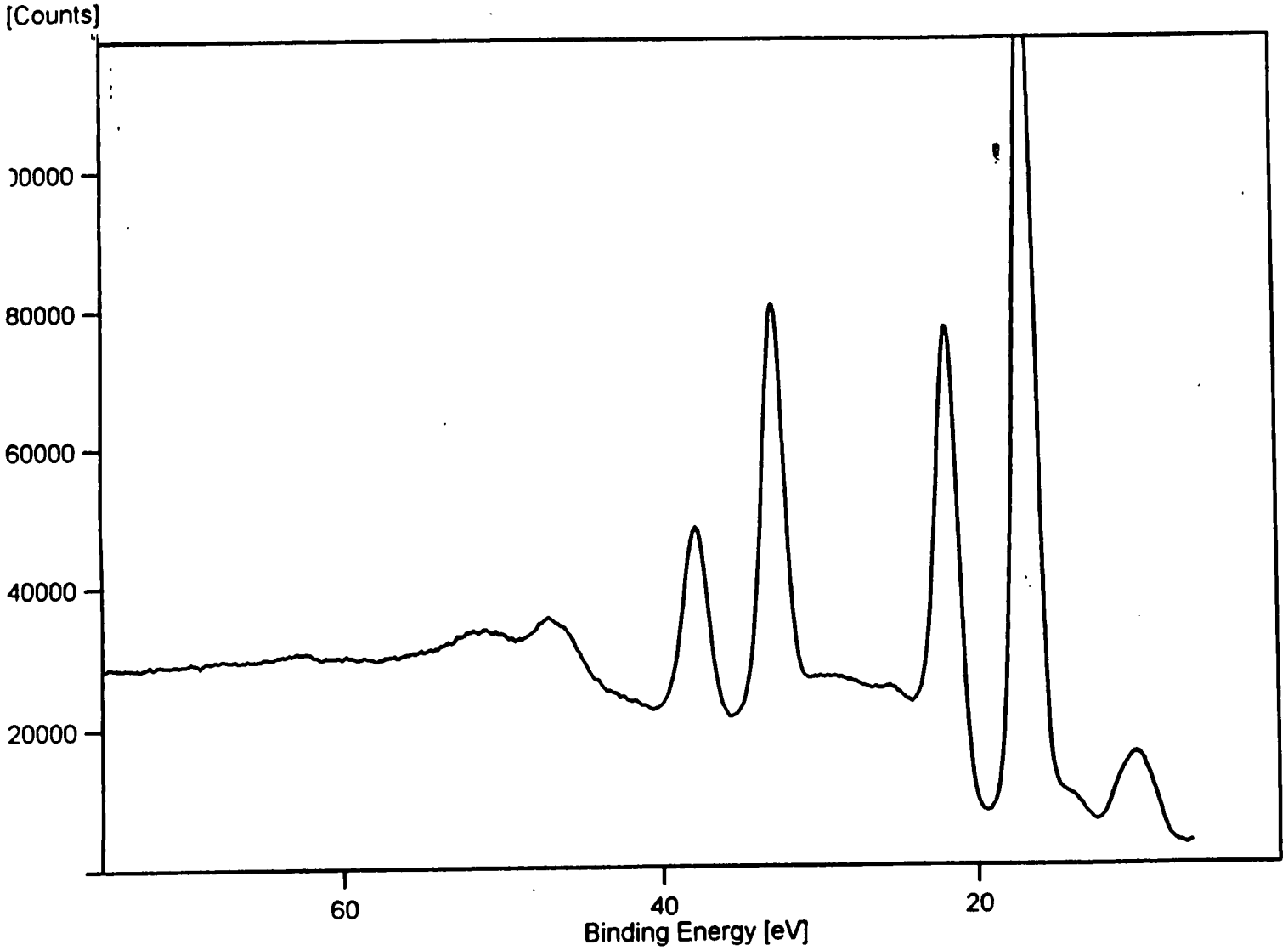
[Counts]
00000
80000
60000
40000
20000
60
40
20
Binding Energy [eV]

Fig. 10

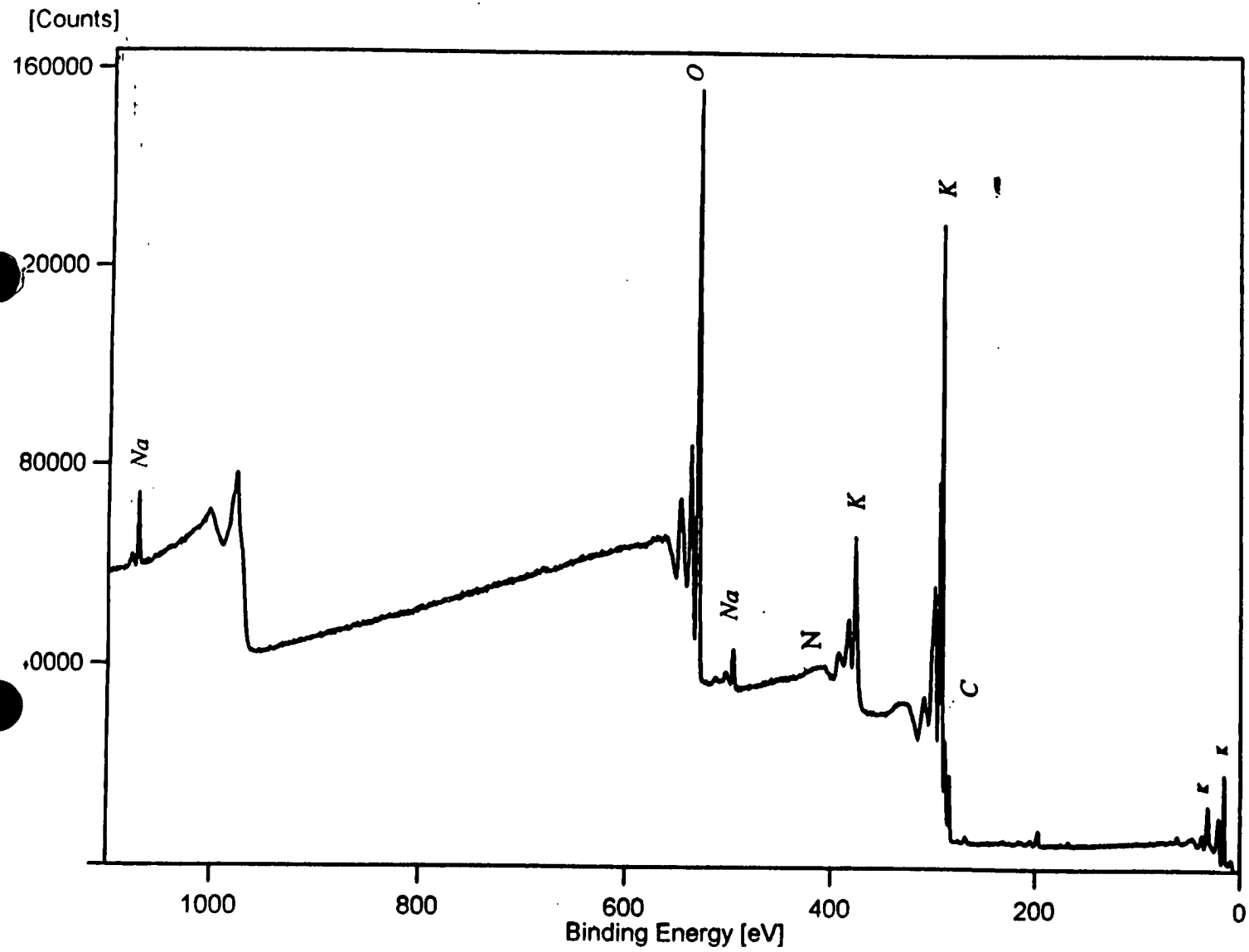
[Counts]
160000
20000
80000
,0000
Na
O
Na
N
K
K
C
1000
800
600
400
200
0
Binding Energy [eV]

Fig. 11

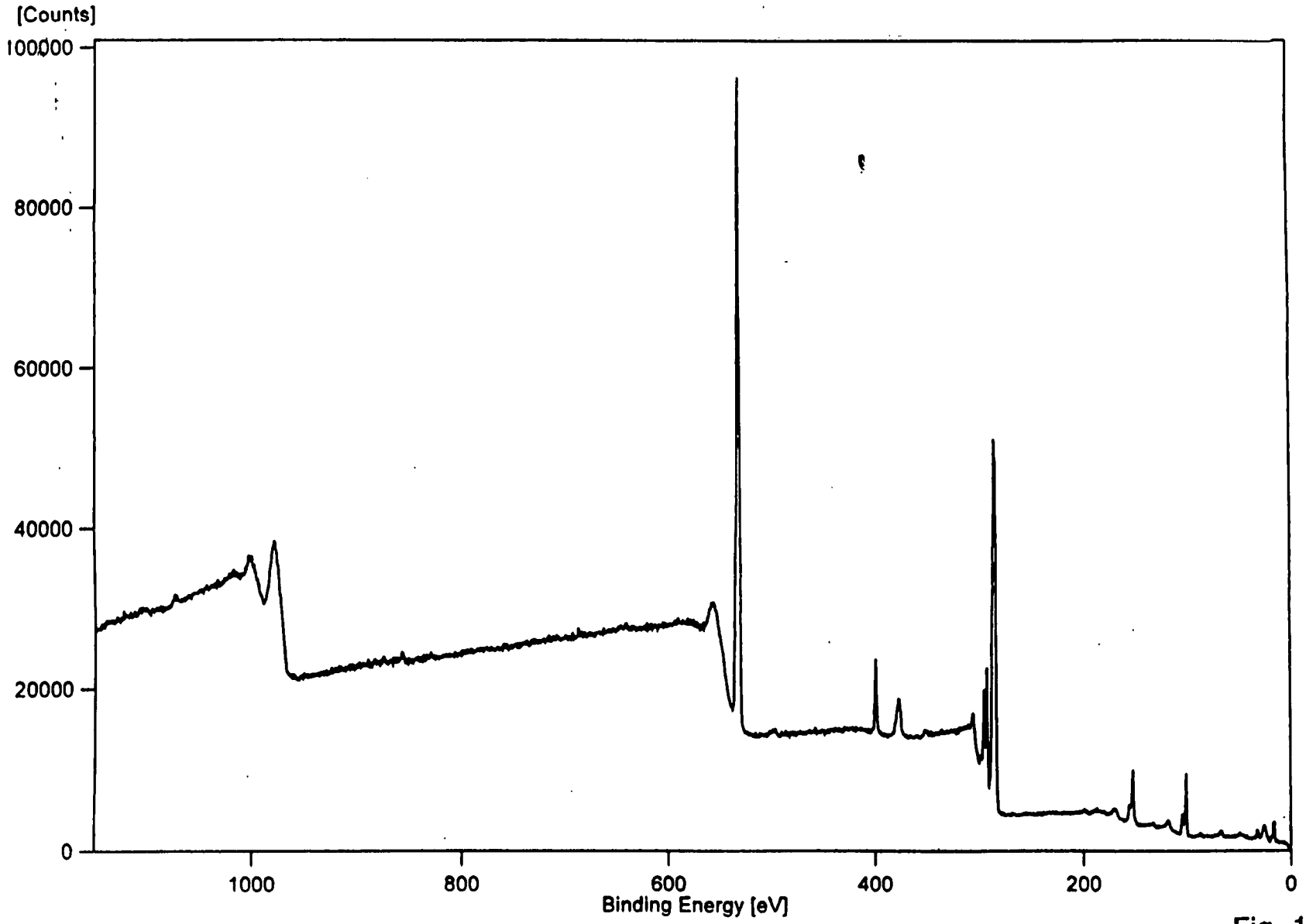
[Counts]
100000
80000
60000
40000
20000
0
1000
800
600
400
200
0
Binding Energy [eV]

Fig. 12

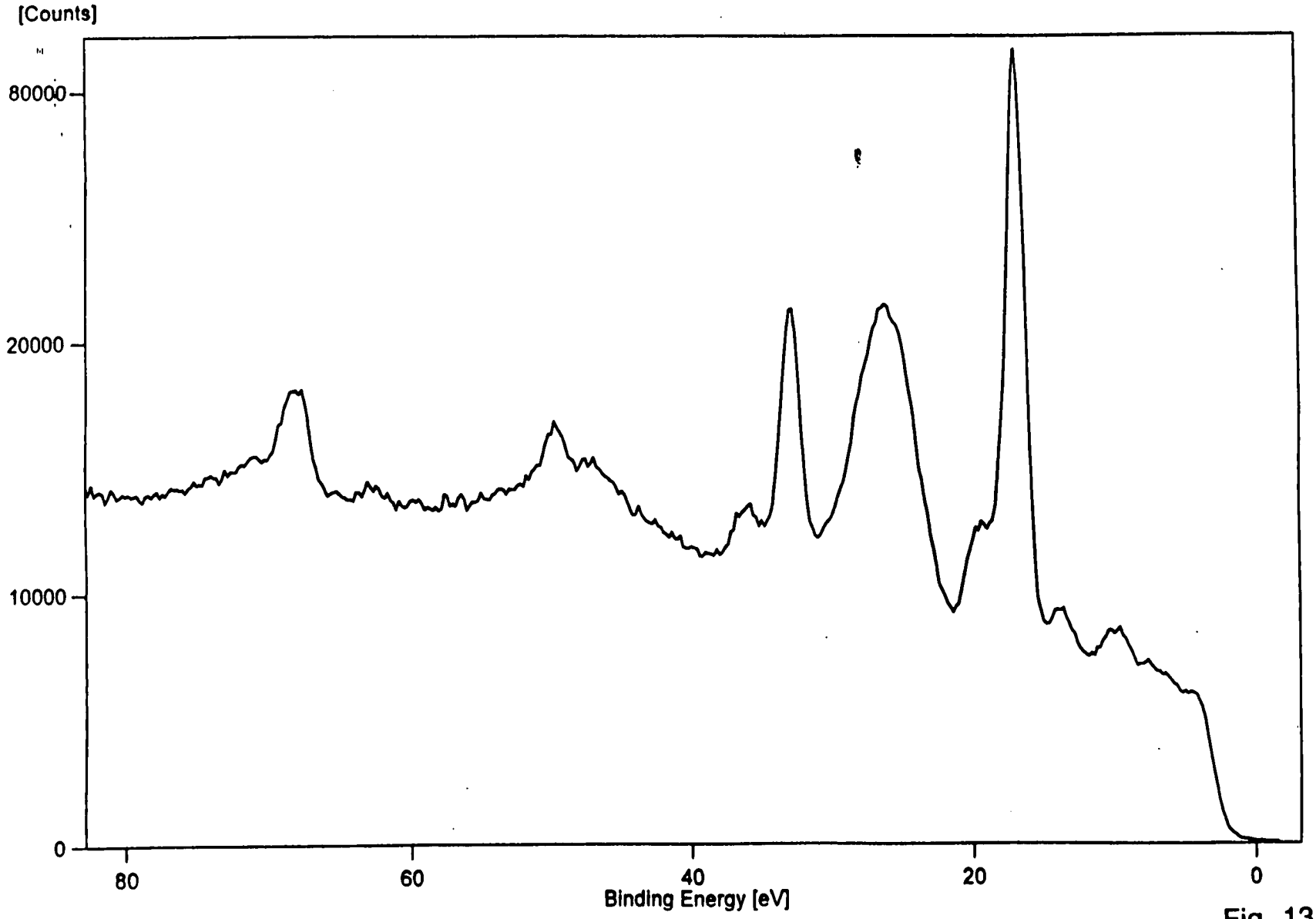

Fig. 13

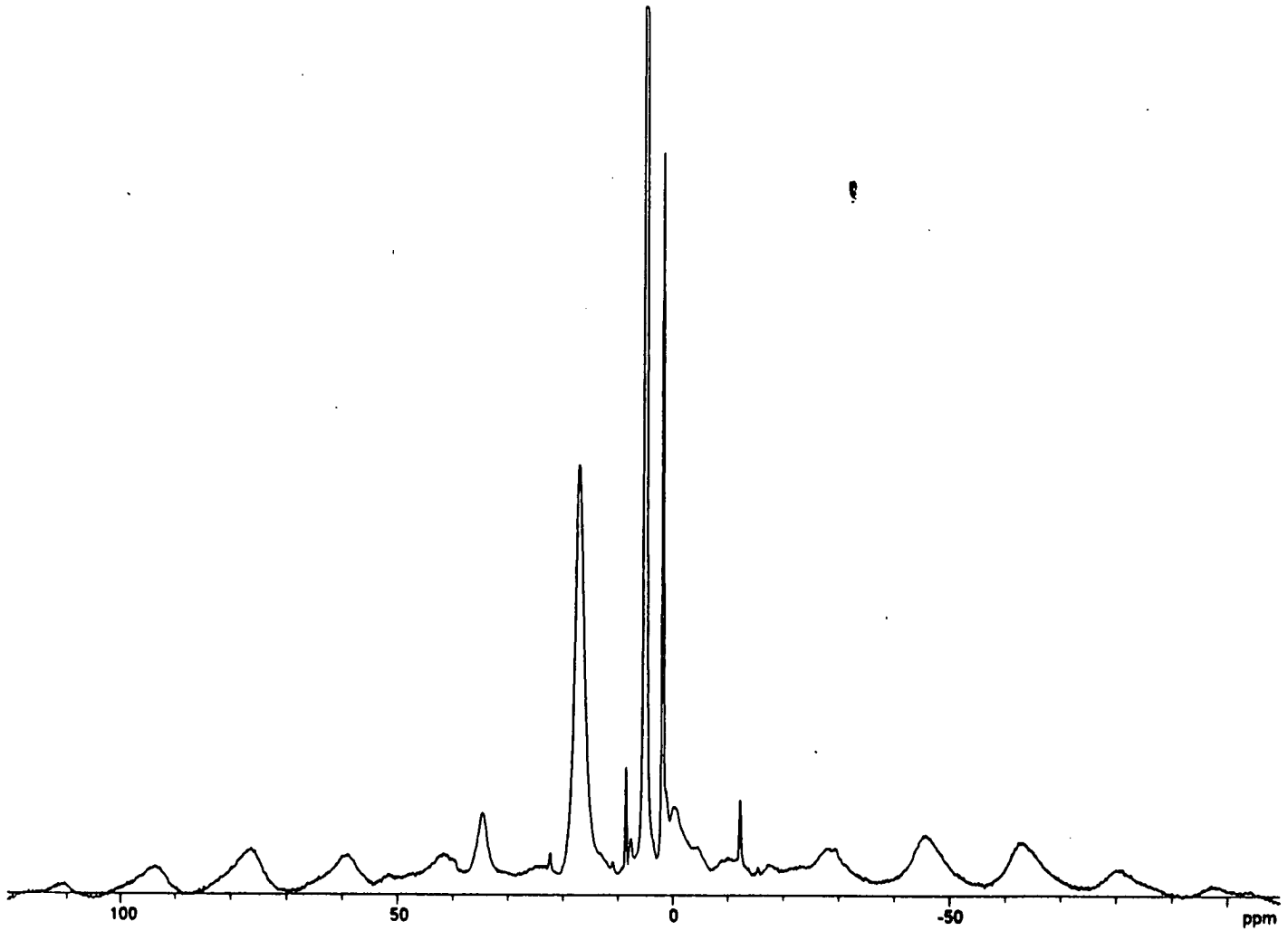

Fig. 14

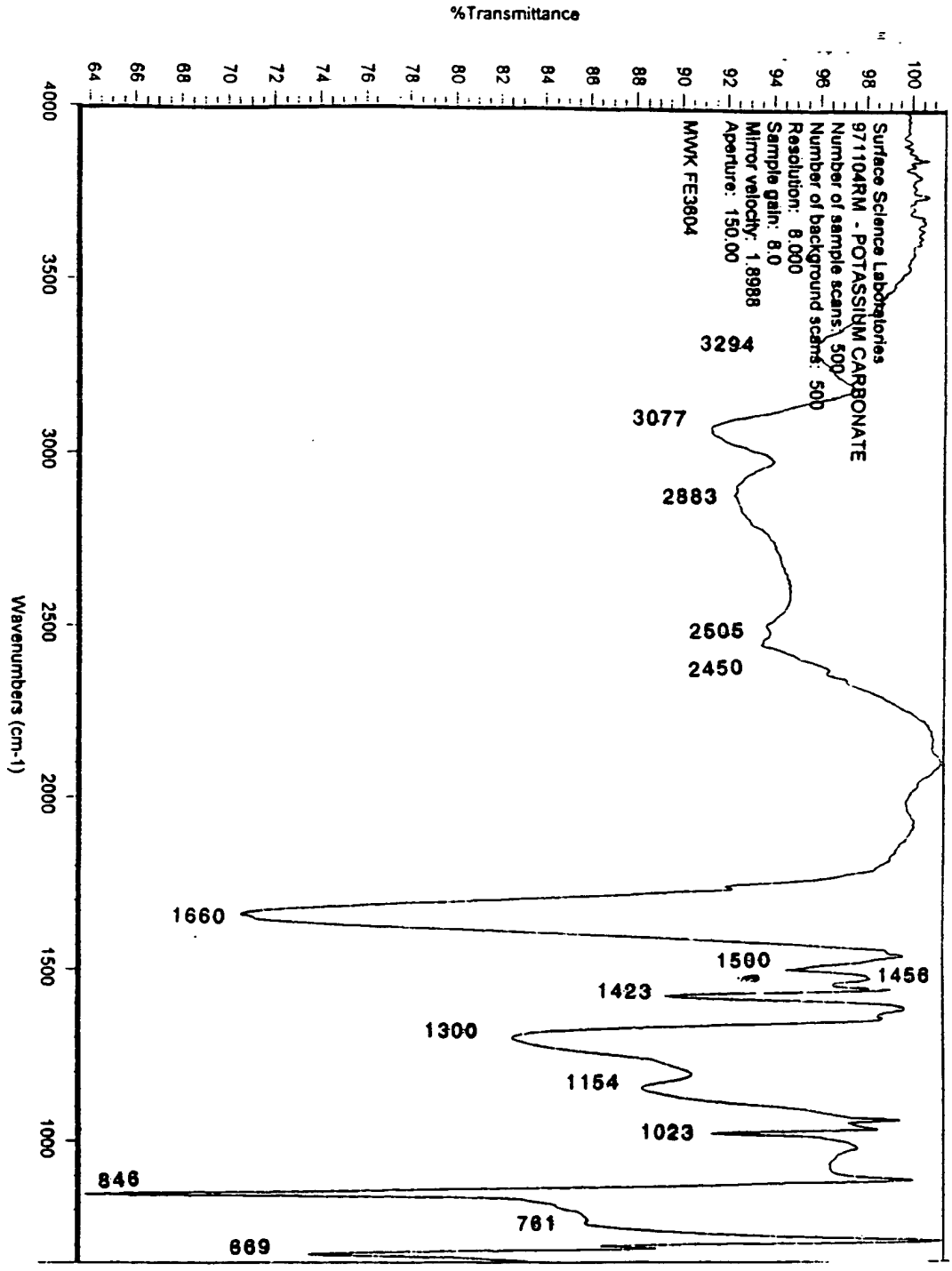
%Transmittance
Wavenumbers (cm-1)
Surface Science Laboratories
971104RM - POTASSIUM CARBONATE
Number of sample scans: 500
Number of background scans: 500
Resolution: 8.000
Sample gain: 8.0
Mirror velocity: 1.8988
Aperture: 150.00
MWK FE3604
3294
3077
2883
2505
2450
1660
1590
1456
1423
1300
1154
1023
846
761
669

Fig. 15

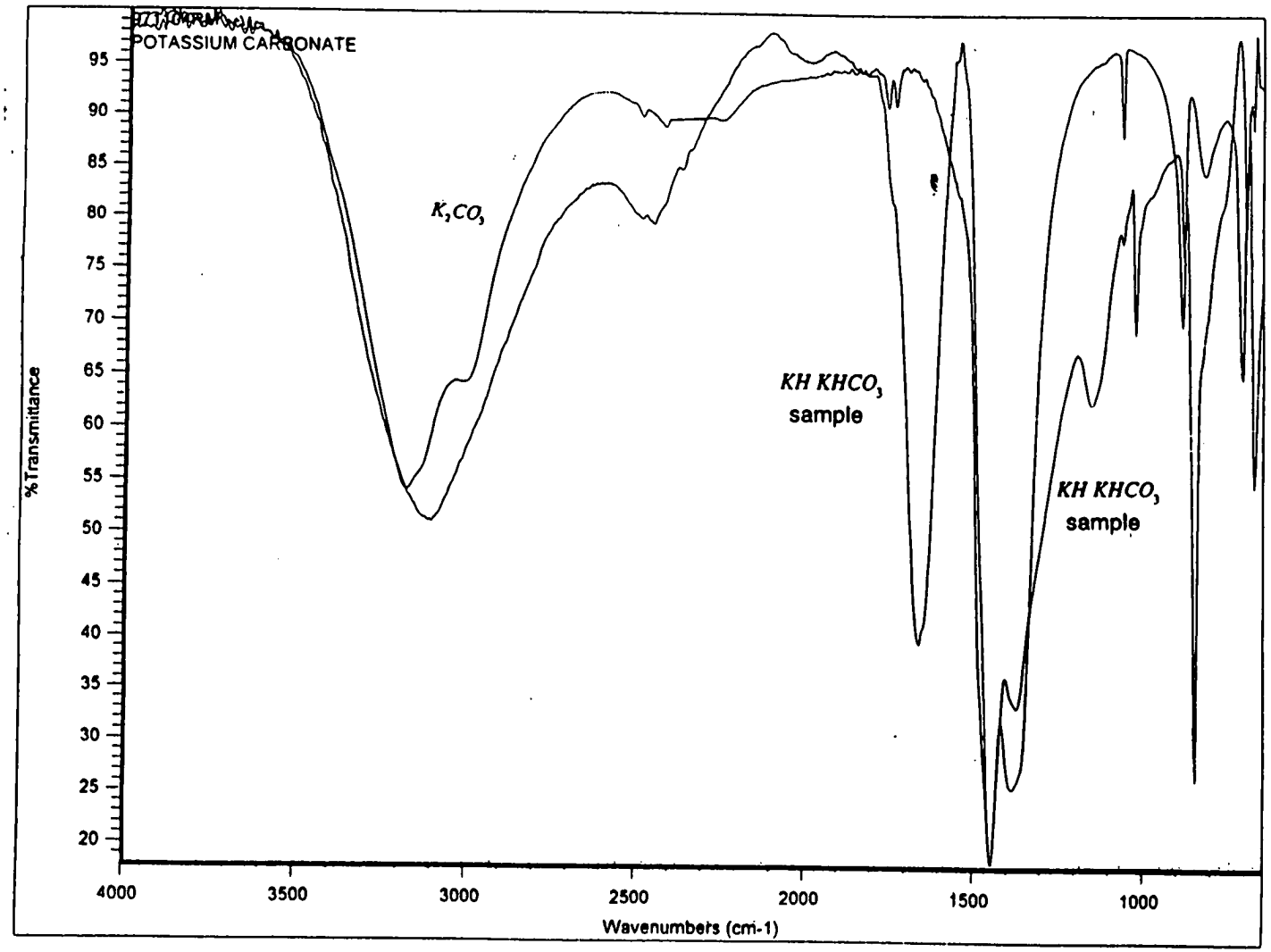
POTASSIUM CARBONATE
K_2CO_3
KH $KHCO_3$
sample
KH $KHCO_3$
sample
%Transmittance
95
90
85
80
75
70
65
60
55
50
45
40
35
30
25
20
4000
3500
3000
2500
2000
1500
1000
Wavenumbers (cm-1)

Fig. 16

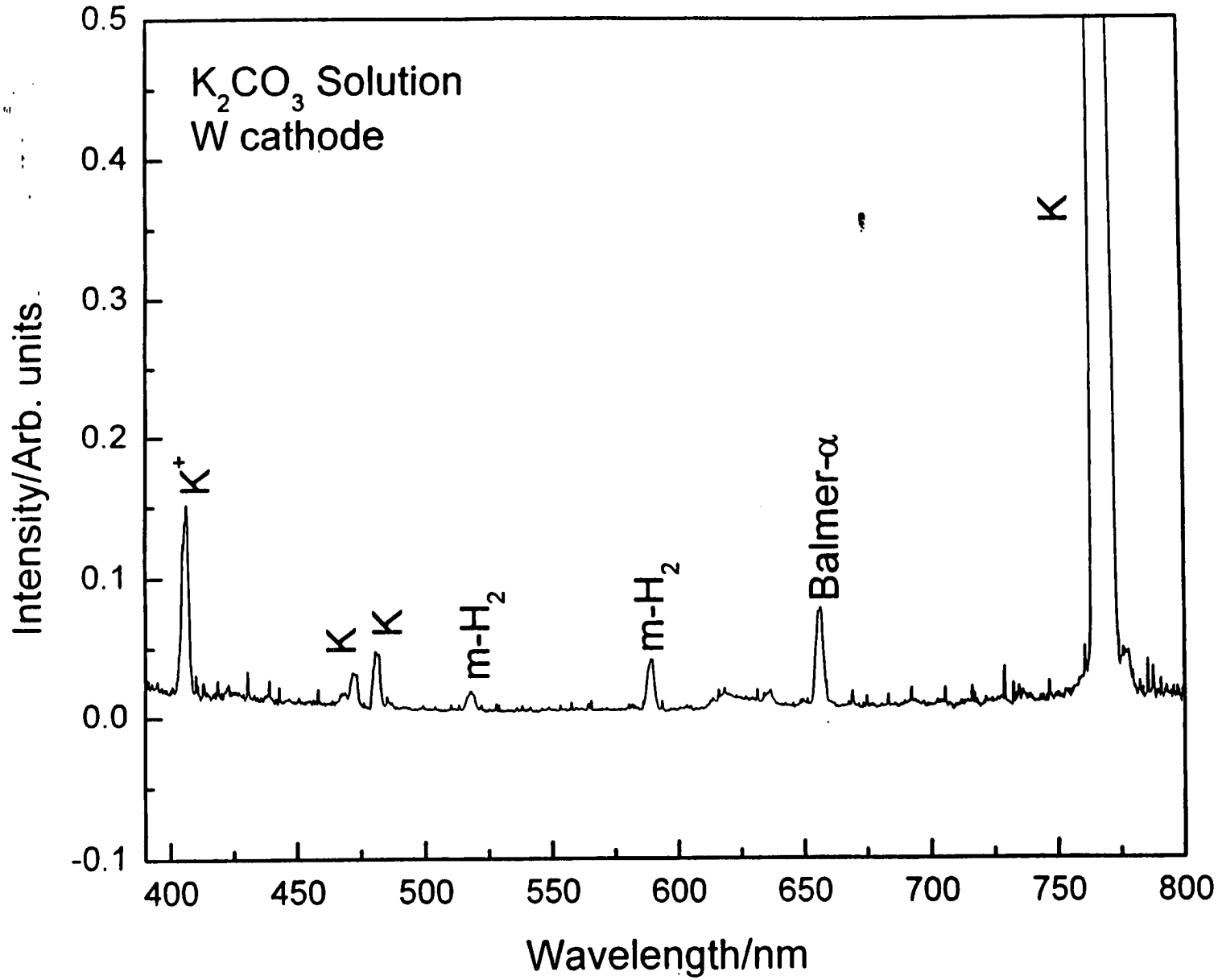
K_2CO_3 Solution
W cathode
Intensity/Arb. units
Wavelength/nm
0.5
0.4
0.3
0.2
0.1
0.0
-0.1
400
450
500
550
600
650
700
750
800
K^+
K
K
m-H_2
m-H_2
Balmer-α
K

Fig. 17

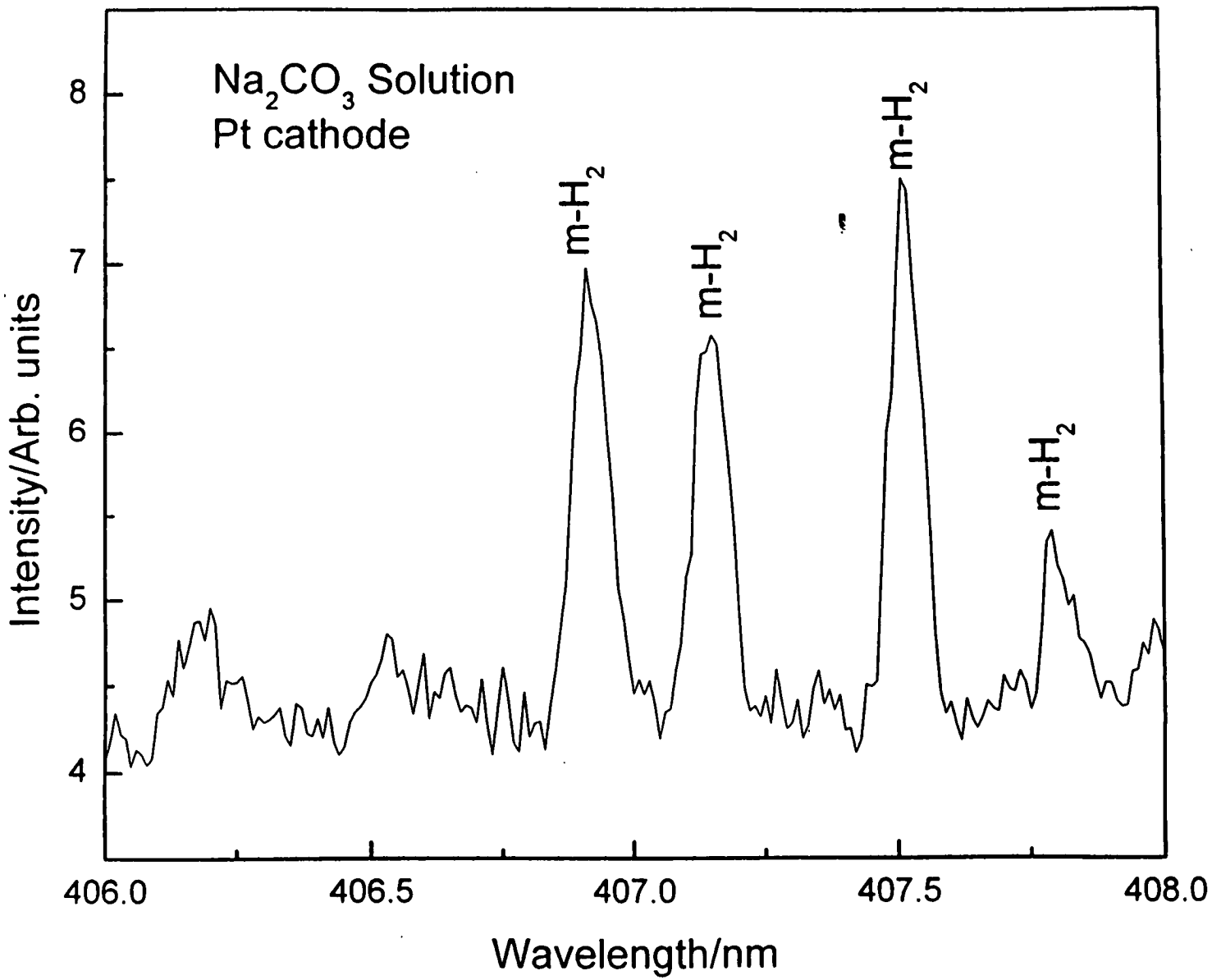
Na2CO3 Solution
Pt cathode
m-H2
m-H2
m-H2
m-H2
Intensity/Arb. units
8
7
6
5
4
406.0
406.5
407.0
407.5
408.0
Wavelength/nm

Fig. 18

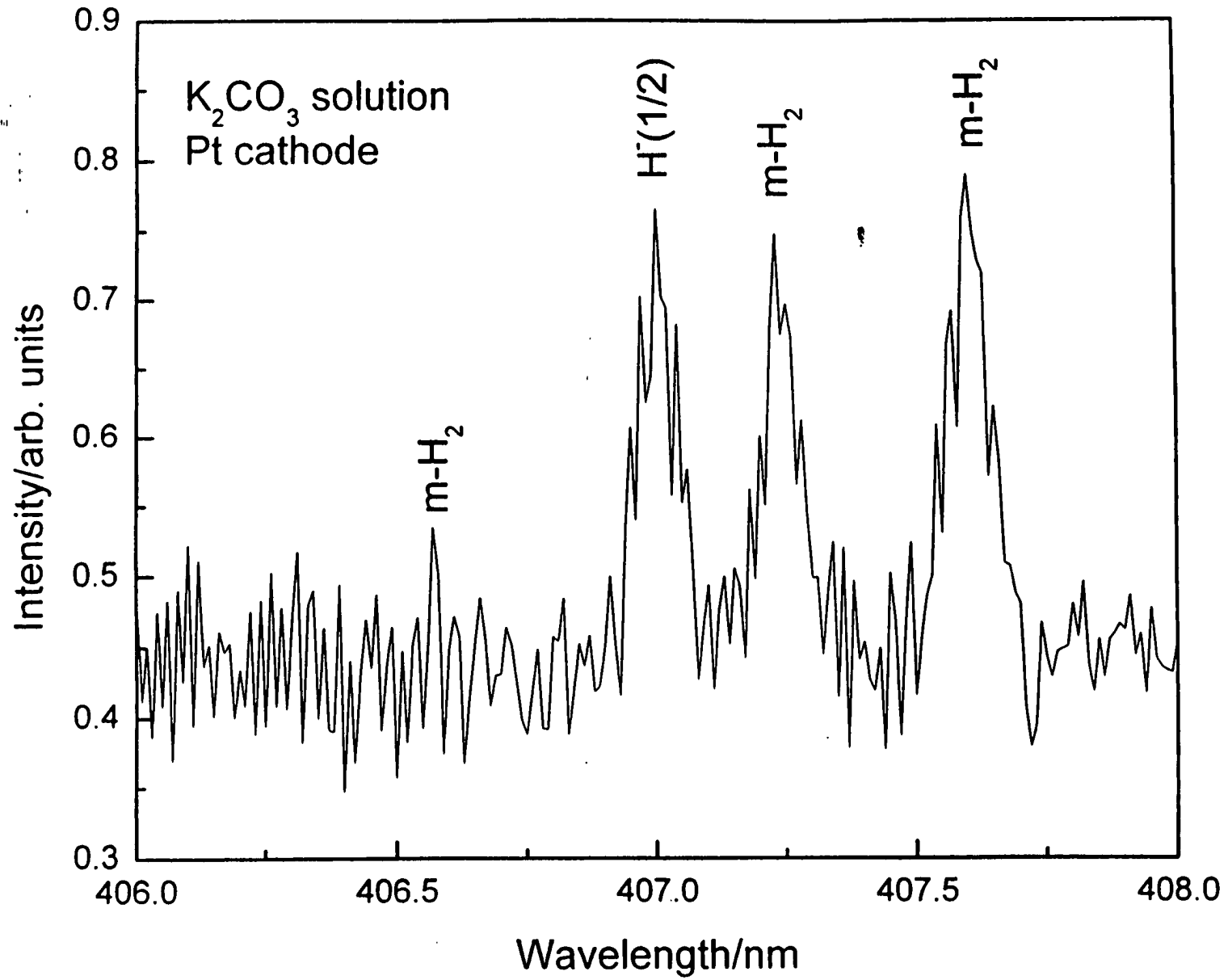
K_2CO_3 solution
Pt cathode
m-H_2
H(1/2)
m-H_2
m-H_2
Intensity/arb. units
0.9
0.8
0.7
0.6
0.5
0.4
0.3
406.0
406.5
407.0
407.5
408.0
Wavelength/nm

Fig. 19

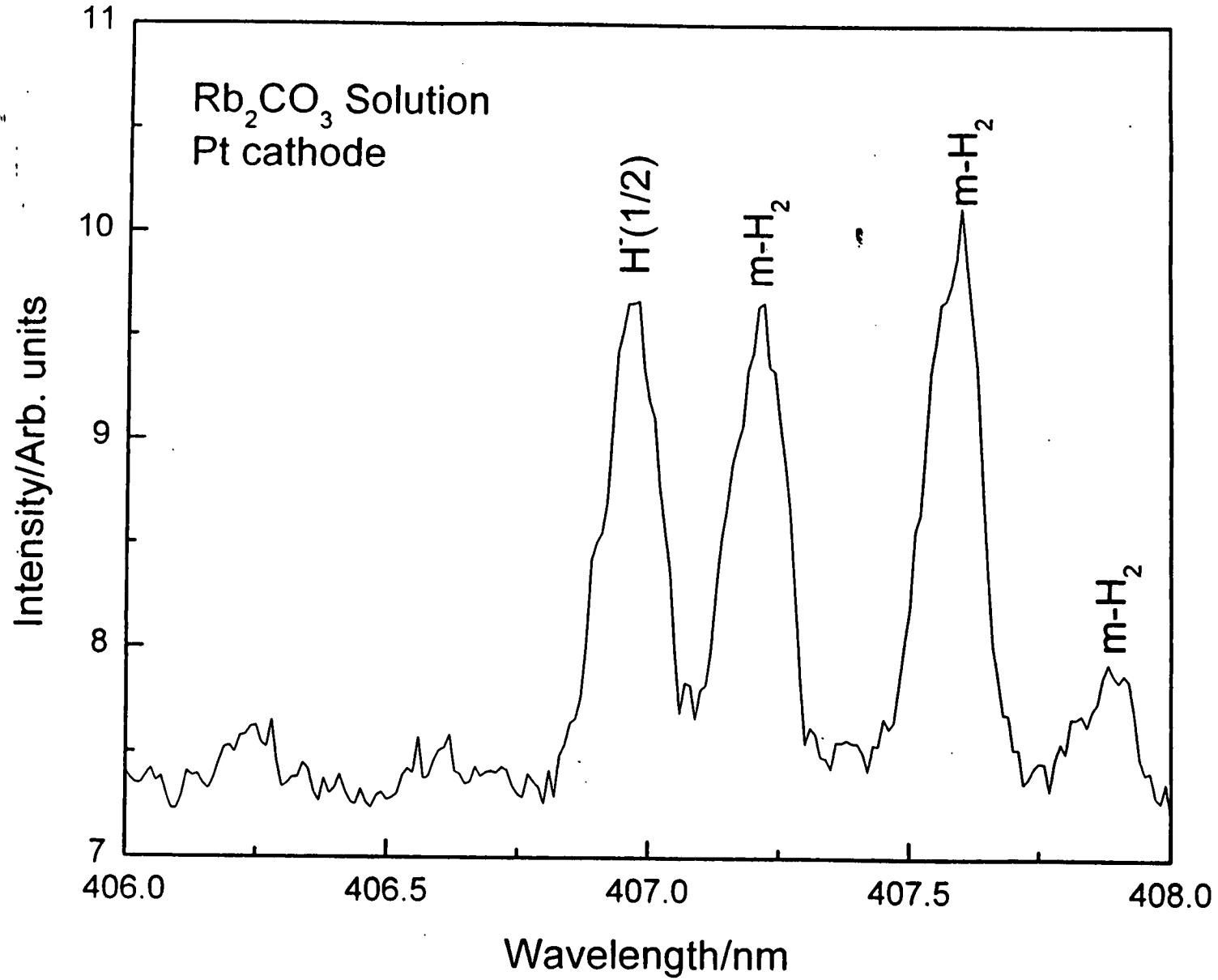
Rb2CO3 Solution
Pt cathode
H(1/2)
m-H2
m-H2
m-H2
Intensity/Arb. units
Wavelength/nm
11
10
9
8
7
406.0
406.5
407.0
407.5
408.0

Fig. 20

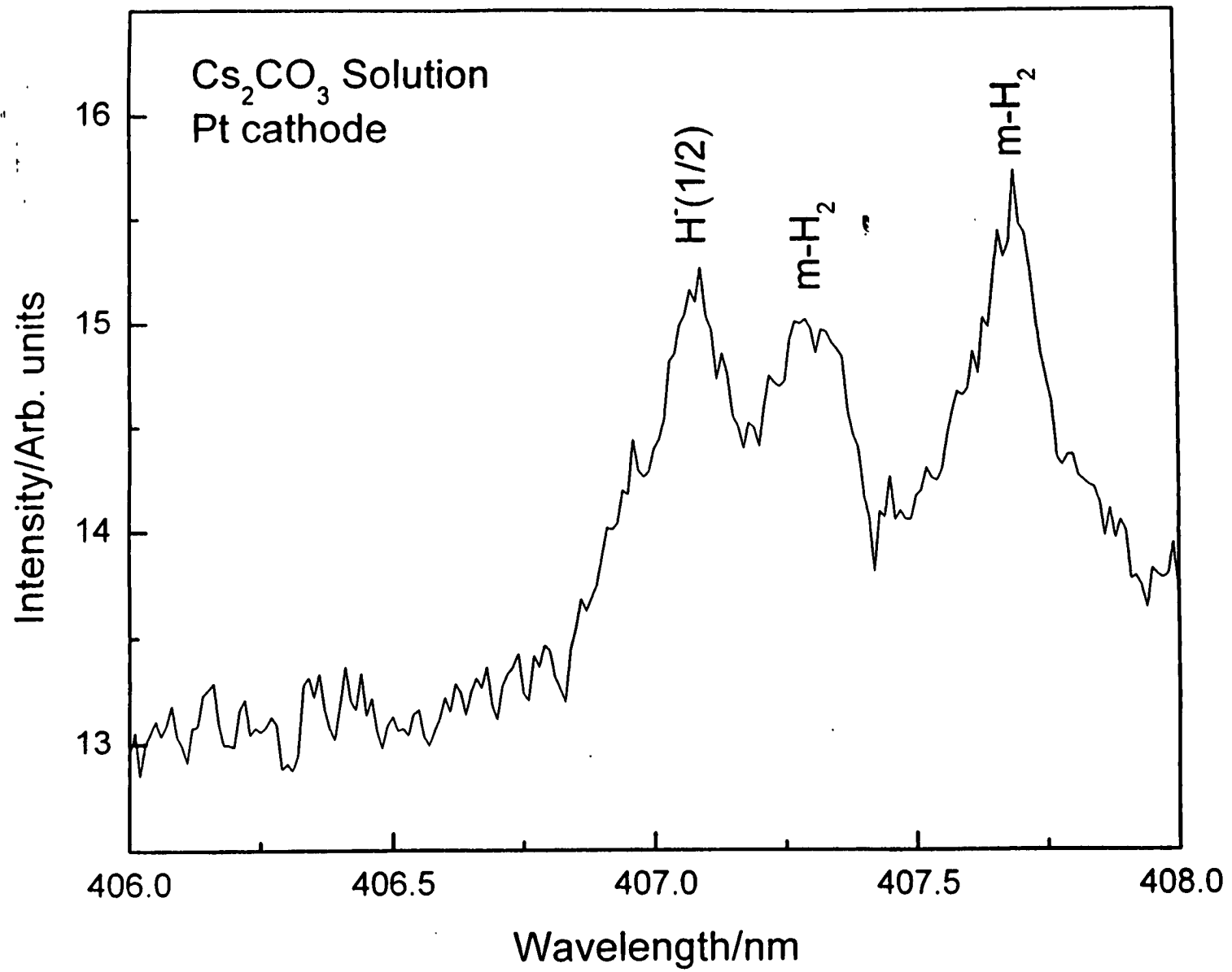
Cs2CO3 Solution
Pt cathode
H(1/2)
m-H2
m-H2
Intensity/Arb. units
16
15
14
13
406.0
406.5
407.0
407.5
408.0
Wavelength/nm

Fig. 21

Table I. The respective hydride compounds and mass assignments (m/z) of the positive ToF-SIMS of the $KH\,KHCO_3$ electrolytic cell sample.

Hydrino Hydride Compound or Fragment	Nominal Mass m/z	Observed m/z	Calculated m/z	Difference Between Observed and Calculated m/z
KH	40	39.97	39.971535	0.0015
K_2H	79	78.940	78.935245	0.004
$(KH)_2$	80	79.942	79.94307	0.001
$KHKOH_2$	97	96.945	96.945805	0.0008
$KH_2(KH)_2$	121	120.925	120.92243	0.003
$KH\,KHCO_2$	124	123.925	123.93289	0.008
KH_2KHO_4	145	144.92	144.930535	0.010
$K(KOH)_2$	151	150.90	150.8966	0.003
$KH(KOH)_2$	152	151.90	151.904425	0.004
$KH_2(KOH)_2$	153	152.90	152.91225	0.012
$K[KH\ KHCO_3]$	179	178.89	178.8915	0.001
$KCO(KH)_3$	187	186.87	186.873225	0.003
$K_2OHKHKOH$	191	190.87	190.868135	0.002
$KH_2KOHKHKOH$	193	192.89	192.883785	0.006
$K_3O(H_2O)_4$	205	204.92	204.92828	0.008
$K_2OH[KH\ KHCO_3]$	235	234.86	234.857955	0.002
$K[H_2CO_4\ KH\ KHCO_3]$	257	256.89	256.8868	0.003
$K_3O[KH\ KHCO_3]$	273	272.81	272.81384	0.004
$[KH_2CO_3]_3$	303	302.88	302.89227	0.012
$K[KH\ KHCO_3K_2CO_3]$	317	316.80	316.80366	0.004
$K[KH\ KHCO_3]_2$	319	318.82	318.81931	0.001
$KH_2[KH\ KOH]_3$	329	328.80	328.7933	0.007
$KOH_2[KH\ KHCO_3]_2$	337	336.81	336.82987	0.020
$KH\,KO_2$ $[KH\ KHCO_3][KHCO_3]$	351	350.81	350.80913	0.001
$KKHK_2CO_3$ $[KH\ KHCO_3]$	357	356.77	356.775195	0.005

$KKH[KH\ KHCO_3]_2$	359	358.78	358.790845	0.011
$K_2OH[KH\ KHCO_3]_2$	375	374.78	374.785755	0.005
$K_2OH[KHKOH]_2$ $[KHCO_3]$	387	386.75	386.76238	0.012
$KKH_3KH_5[KH\ KHCO_3]_2$	405	404.79	404.80933	0.019
$K_3O[K_2CO_3]$ $[KH\ KHCO_3]$ or $K[KH\ KOH(K_2CO_3)_2]$	411	410.75	410.72599	0.024
$K_3O[KH\ KHCO_3]_2$	413	412.74	412.74164	0.002
$K\begin{bmatrix} KH\ KOH \\ (KH\ KHCO_3)_2 \end{bmatrix}$	415	414.74	414.75729	0.017
$KH_2OKHCO_3[KH\ KHCO_3]_2$	437	436.81	436.786135	0.024
$KKHKCO_2[KH\ KHCO_3]_2$	442	441.74	441.744375	0.004
$K[KH\ \ KHCO_3]_3$	459	458.72	458.74711	0.027
$H[KH\ KOH]_2[K_2CO_3]_2$ or $K_4O_2H[KH\ KHCO_3]_2$	469	468.70	468.708085	0.008
$K[K_2CO_3][KHCO_3]_3$	477	476.72	476.744655	0.025
$K_2OH[KH\ KHCO_3]_3$	515	514.72	514.713555	0.006
$K_3O[KH\ KHCO_3]_3$	553	552.67	552.66944	0.001
$K[KH\ \ KHCO_3]_4$	599	598.65	598.67491	0.025
$K_2OH[KH\ KHCO_3]_4$	655	654.65	654.641355	0.009
$K_3O[KH\ KHCO_3]_4$	693	692.60	692.59724	0.003
$K[KH\ \ KHCO_3]_5$	739	738.65	738.60271	0.047
$K_3O[KH\ KHCO_3]_5$	833	832.50	832.52504	0.025
$K[KH\ \ KHCO_3]_6$	879	878.50	878.53051	0.031
$K_3O[KH\ KHCO_3]_6$	973	972.50	972.45284	0.047

Table II. The binding energies of XPS peaks of K_2CO_3 and the $KH\,KHCO_3$ electrolytic cell sample.

XPS #	$C\ 1s$ (eV)	$O\ 1s$ (eV)	$K\ 3p$ (eV)	$K\ 3s$ (eV)	$K\ 2p_3$ (eV)	$K\ 2p_1$ (eV)	$K\ 2s$ (eV)
K_2CO_3	288.4	532.0	18	34	292.4	295.2	376.7
$KH\,KHCO_3$ Electrolytic Cell Sample	288.5	530.4 537.5 547.8	16.2 22.8	32.1 38.8	291.5 298.5	293.7 300.4	376.6 382.6
Min	280.5	529			292		
Max	293	535			293.2		

Table III. The NMR peaks of the $KH\,KHCO_3$ electrolytic cell sample with their assignments.

Peak at Shift (ppm)	Assignment
+34.54	side band of +17.163 peak
+22.27	side band of +5.066 peak
+17.163	$KH\,KHCO_3$
+10.91	$KH\,KHCO_3$
+8.456	$KH\,KHCO_3$
+7.50	$KH\,KHCO_3$
+5.066	H_2O
+1.830	$KH\,KHCO_3$
-0.59	side band of +17.163 peak
-12.05	$KH\,KHCO_3$ [a]
-15.45	$KH\,KHCO_3$

[a] small shoulder is observed on the -12.05 peak which is the side band of the +5.066 peak

Table IV. Alkali emission lines recorded on plasma electrolysis cells.

Plasma Electrolysis Electrolyte	Alkali Metal (M) Emission (nm)	M^+ Emission (nm)	M^{2+} Emission (nm)
Na_2CO_3	497.9 498.3 589 589.6 819.5	None	None
K_2CO_3	766.5 769.9	404.3	None
Rb_2CO_3	794.7 780 761.9	408.4	None
Cs_2CO_3	852.1 894.3	None	404.5